Mon. Not. R. Astron. Soc. **000**, 1–19 (2013) Printed 6 September 2013 (MN LATEX style file v2.2)

Particle acceleration and dynamics of double-double radio galaxies: theory vs. observations

C. Konar[1] ⋆ and M.J. Hardcastle[2]
[1] *Institute of Astronomy and Astrophysics, Academia Sinica, National Taiwan University, Taipei 10617, Taiwan, R.O.C.*
[2] *School of Physics, Astronomy and Mathematics, University of Hertfordshire, College Lane, Hatfield*

Accepted. Received

ABSTRACT
In this paper we show that a small sample of radio galaxies with evidence for multiple epochs of jet activity (so-called 'double-double' radio galaxies) have the same electron injection spectral index in the two activity episodes, a result which might be considered surprising given the very different lobe dynamics expected in the first and second episode. We construct models for the dynamics of radio galaxies, with an emphasis on their episodic behaviour, and show that hotspot formation and confinement of lobes for the inner double of double-double radio galaxies are possible even without any thermal matter in the outer cocoon. We argue that (i) the observed similar injection spectral indices are due to similar jet powers in the two episodes, (ii) the 'spectral index–radio power' correlation of a flux limited sample of radio galaxies is the primary one, and not the 'spectral index–redshift correlation', (iii) jets are made of pair plasma and not electron-proton, (iv) and the Lorentz factor of the spine of the jet should be $\gtrsim 10$ to explain the observations. Furthermore, we argue that the observations show that higher power radio galaxies do not have a higher jet bulk Lorentz factors, but instead simply have a higher number density of particles in the jet rest frame. A consequence of our models is that aligned double-double radio galaxies with very old ($\gtrsim 10^8$ yr) outer doubles, or misaligned double-double radio galaxies, are statistically more likely to have dissimilar injection indices in two different episodes, as they will probably have different jet powers.

Key words: Radiation mechanisms: nonthermal – Radio continuum: galaxies – Galaxies: active

1 INTRODUCTION

Observations suggest (Richstone et al. 1998) that every massive galaxy harbours a super-massive black hole (SMBH). Under favourable conditions, the black hole and its surrounding accretion system can launch relativistic jets carrying charged sub-atomic particles (e.g., e^-p^+ or e^-e^+) together with magnetic fields. These jets supply particles and energy to lobes inflated by the jets themselves, which may extend from kpc to Mpc scales. The complete system, consisting of a SMBH at the centre of a galaxy, the jets, and the lobes, is called a radio galaxy, and comparatively powerful jets give rise to Fanaroff-Riley type II (FR II) radio galaxies (Fanaroff & Riley 1974). Observations have proven (e.g. Schoenmakers et al. 2000) that the phenomenon of launching jets is episodic in nature (see the right panel of Fig. 1 for images of an episodic radio galaxy) with the duration of the quiescent phase ranging from a tenth of a Myr to a few tens of Myr in several well-studied cases (Konar et al. 2012, 2013). The speed of the jets in FR II radio galaxies is known to be supersonic with respect to the internal sound/magnetosonic speed of the lobe as well as the jet fluid, and so the jet inevitably terminates in a shock called the jet-termination shock (JTS). The observed bright radio features at the end of the lobes, which are known as hotspots, are identified with the JTS (see Fig. 1 for schematic picture of a radio galaxy). At the JTS, some fraction of the kinetic energy of the jet is put into a population of relativistic particles at the shock by a process known as Diffusive Shock Acceleration (DSA, see Bell 1978a, 1978b; Kirk et al. 2000) before the particles escape from the shock/hotspot region and expand into the lobes. In the FRII radio galaxies, the relativistic DSA gives rise to a power-law energy distribution of the particles in the hotspots, which is given by $N(E) \propto E^{-\delta}$, where $N(E)$ is the number of particles at energy E and δ is the power-law index. The leptons in the jet, being lighter particles, are efficiently accelerated at the hotspots and radiate via the synchrotron process; protons, being much more massive, may still be accelerated but produce negligible amounts of radiation by this mechanism. Since the energy distributions of the relativistic particles are power laws, the synchrotron spectra from regions of FR II RGs where particle acceleration has recently taken place are also expected to be power laws with the general form $S(\nu) = S_0\nu^{-\alpha_{\rm inj}}$, where $S(\nu)$ is the synchrotron flux den-

⋆ E-mail: chiranjib.konar@gmail.com (CK)

sity from a given emission region of the lobes and/or hotspots, S_0 is the normalization and $\alpha_{\rm inj}$ is the injection spectral index (hereafter injection index). The index, $\alpha_{\rm inj}$ is related to the power-law index of energy distribution, δ by $\alpha_{\rm inj} = (\delta - 1)/2$ (Pacholczyk 1980). In principle, the injection index $\alpha_{\rm inj}$ can give us information about the properties of the JTS[1]. The actual observed spectra of large-scale regions of these RGs are more complex, because of the effects of radiative and inverse-Compton losses and adiabatic expansion, which give rise to broken or curved synchrotron spectra (e.g. Heavens & Meisenheimer 1987, Jaffe & Perola 1973) and so in general measurements at several frequencies are needed to determine the injection index.

The main objectives of the present paper are (i) to study observationally the behaviour of $\alpha_{\rm inj}$ in two different episodes of jet formation activity of individual episodic radio galaxies, (ii) to study the dynamics of jets, especially the inner jets of episodic radio galaxies, and (iii) to try to determine the parameters of the system on which $\alpha_{\rm inj}$ depends. By doing so we can learn a good deal about the properties of radio galaxies in general.

The remainder of the paper is structured as follows. In Section 2 we construct a small sample of episodic radio galaxies from the literature and our own observations. Section 3 describes how we have measured the injection indices for the multiple epochs of the sample of episodic radio galaxies, and how we estimate jet power for these sources; we then present the key observational results of this paper, including a strong correlation between the injection indices seen in the two epochs of the episodic radio galaxy activity. In Section 4 we move on to discuss relativistic models for radio galaxy dynamics, and their implications for the expected properties of JTS and injection index in episodic radio galaxies. Section 5 then discusses our observational results in the context of these models. Our conclusions are given in Section 6.

2 SAMPLE COMPILATION, OBSERVATIONS AND DATA REDUCTION

We have compiled from the literature a sample of 8 known double-double radio galaxies (DDRGs), which are listed in Table 1. By definition, these objects show two episodes of jet forming activity. Out of the 8 sample objects, we obtained new radio observations for 4 DDRGs (J0041+3224, J0116-4722, J1158+2621 and J1835+6204) with the GMRT at 150, 240, 332, 605 and 1287 MHz and used archival VLA data at higher frequencies to estimate the injection indices. The observing logs, the method of observations and the data reduction for these objects are discussed in detail by Konar et al. (2012; 2013). From the literature, we compiled flux densities down to very low frequencies to constrain the radio spectra of the outer doubles of these 4 DDRGs. The remaining 4 objects in our sample already had published estimates of $\alpha_{\rm inj}$ for both the inner and outer doubles, and we adopt those values in this paper.

[1] Although observations of high-energy synchrotron radiation (e.g. Meisenheimer et al. 1989; Hardcastle et al. 2004) demonstrate that the hotspots are locations of high-energy particle acceleration, it is important to note that we cannot rule out the possibility of particle acceleration elsewhere in the sources. In particular, observations of emission from the jets, in some cases possibly extending to X-ray energies (e.g. Wilson et al. 2001), suggest that particles are (re)accelerated in the jet regions, before the JTS. The acceleration mechanism here is uncertain, but cannot be the result of jet-wide shocks stationary in the galaxy frame, which would make the downstream jet subsonic; some smaller-scale process must be responsible for the particle acceleration allowing emission to be seen from the jets. In this paper we make the assumption that the hotspots (the JTS), rather than the jets, are the location at which the bulk of the particle acceleration occurs, since it seems very likely that they are the location at which the bulk of the jet kinetic energy is thermalized; as we will argue later in the paper, a self-consistent model can be generated in which there is little bulk deceleration of the jet before the JTS. We are not aware of any direct method of testing this assumption.

Table 1. Injection index of inner and outer doubles for our DDRG sample. Columns are as follows. Column 1: source name, Column 2: $\alpha_{\rm inj}$ with error of the inner double, Column 3: $\alpha_{\rm inj}$ with error of the outer double, and Column 4: reference to the source of $\alpha_{\rm inj}$ and comment.

Source	$\alpha_{\rm inj}^{\rm inn}$	$\alpha_{\rm inj}^{\rm out}$	Ref. and comment
(1)	(2)	(3)	(4)
J0041+3224	$0.724^{+0.034}_{-0.041}$	$0.756^{+0.167}_{-0.122}$	a
J0116−4722	$0.700^{+0.100}_{-0.100}$	$0.618^{+0.072}_{-0.065}$	a,b
J0840+2949	$0.830^{+0.050}_{-0.050}$	$0.810^{+0.050}_{-0.050}$	c
J1158+2621	$0.768^{+0.029}_{-0.047}$	$0.788^{+0.038}_{-0.040}$	a
J1352+3126	$0.720^{+0.020}_{-0.020}$	$0.855^{*}{}^{+0.030}_{-0.030}$	d
J1453+3308	$0.566^{+0.051}_{-0.058}$	$0.568^{+0.065}_{-0.060}$	e
J1548−3216	$0.579^{+0.113}_{-0.157}$	$0.567^{+0.070}_{-0.066}$	f
J1835+6204	$0.860^{+0.034}_{-0.488}$	$0.818^{+0.070}_{-0.064}$	a

*: The average $\alpha_{\rm inj}$ of two outer lobes from Joshi et al. (2011).
a: This paper for $\alpha_{\rm inj}$ of the inner double and Konar et al. (2012b, in prep) for $\alpha_{\rm inj}$ of the outer double. b: Saripalli et al. (2002) for the injection index for the inner double. c: Jamrozy et al. (2007). d: Joshi et al. (2011). e : Konar et al. (2006). f: We fitted the inner-double and outer-double spectra, using the data from the Table 2 of Machalski, jamrozy & Konar (2010).

3 SPECTRA, INJECTION INDICES AND JET POWERS

3.1 Injection index

In this section we summarize the method by which $\alpha_{\rm inj}$ was estimated from our new observations. For details of the observations, see Konar et al. (2012, 2013).

The spectra of the inner doubles were constrained from the high-frequency measurements. Most of the inner doubles of our DDRGs are embedded in the diffuse emission of the relic outer lobes. Obviously, the uv data at different frequencies used for imaging have different shortest baselines; so we re-mapped the fields of each DDRG at higher frequencies with the same lower uv cutoff in order to image the inner doubles free from the outer diffuse emission. The high-frequency flux densities and their errors, both for individual components and for the total inner doubles of our sample DDRGs, were measured from the maps re-made with similar lower uv cutoff; these fluxes are tabulated by Konar et al. (2012; 2013). We assumed 7 per cent flux density errors at 0.62 and 1.28 GHz and 5 per cent errors at 1.40, 4.86, 8.46 and 22.46 GHz for our flux density measurements of each inner lobe. The errors on the total flux densities of the inner doubles (without the core) were obtained by propagating the errors of the two individual lobes. No appreciable curvature was visible in the spectra of the individual inner lobes and the core-subtracted total inner doubles of all the DDRGs within our observable frequency range. We therefore constrained $\alpha_{\rm inj}$ of the inner doubles by fitting power laws to their observed integrated spectra. For J0116-4722, there are no high-resolution data at high frequencies except for those at 1376 and 2496 MHz published by Saripalli et al. (2002); for this source we have therefore used these two flux densities to constrain the power-

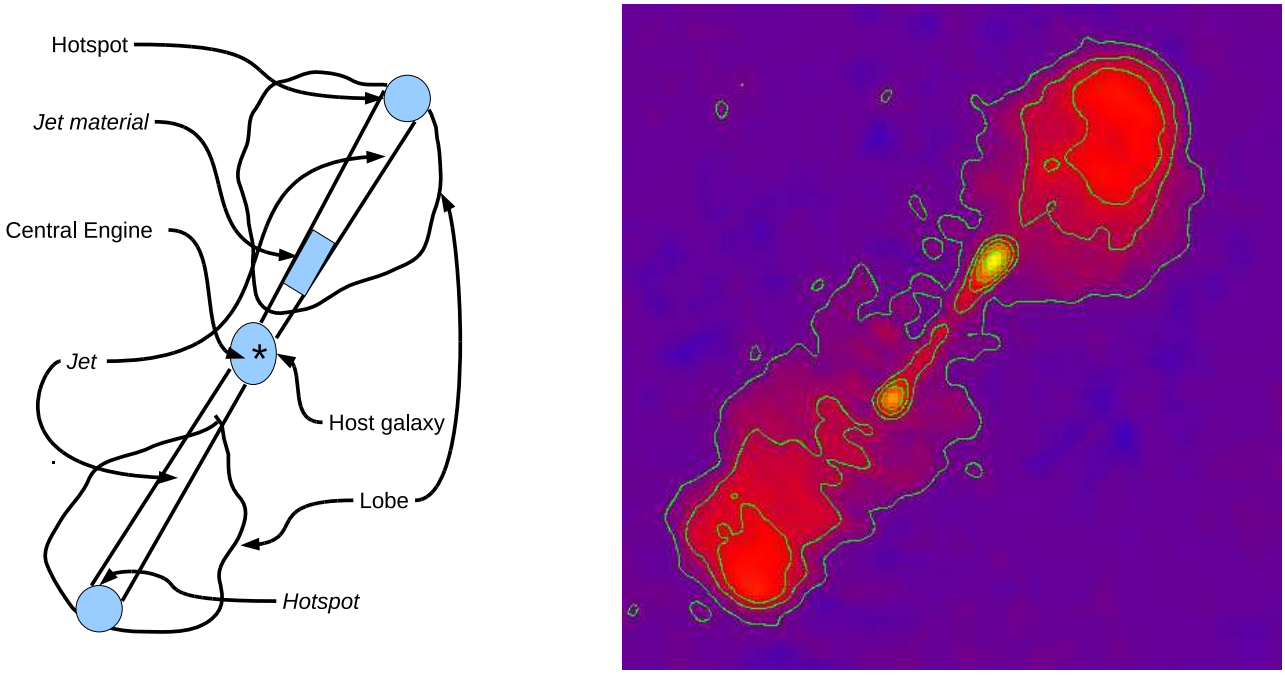

Figure 1. Left panel: A schematic picture of an FR II RG. Only a portion of the continuous jet-fluid is shown in blue. Right panel: A false colour image of a known episodic radio galaxy, J1158+2621 made with the GMRT at L band (Konar et al., 2013).

law spectrum of the inner double of J0116-4722, on the assumption that the spectrum of the inner double of this source is a power law within our observable range (10−22000 MHz). For the outer doubles, by contrast, the spectra have curvature at higher frequencies, presumably due to synchrotron and inverse-Compton losses. However, the low-frequency part of the spectra are still power laws and have not yet been affected by the loss, so that the spectral index of that part of the spectra is presumably a good estimate of $\alpha_{\rm inj}$ (see Konar et al., 2006; 2012; 2013).

3.2 Jet power

The particle acceleration in FRIIs is thought to be due to the JTS at the hotspots. The efficiency of acceleration depends on the JTS strength which is expected to depend on the jet power ($Q_{\rm j}$). The shock strength depends on the upstream speed of the jet as observed from the hotspot frame (i.e. shock frame) which also moves with respect to the host galaxy frame. In a given ambient medium, the hotspot speed depends on the jet power and composition, through momentum balance at the contact discontinuity at the jet head. If the speed of the hotspot alters, the speed of the upstream jet with respect to the hotspot frame also alters (see Section 4.4). Hence, the shock strength and particle acceleration efficiency depends on the jet power, and so in this section we consider methods for estimating this for our target sources.

It is not in practice easy to estimate $Q_{\rm j}$ from observations of the jets themselves, and, even if it were, we would be unable to do so since jets are not easily detectable in our observations. Instead we estimate the jet power by measuring the total enthalpy of the lobes and dividing it by the spectral age of the source, assuming the minimum-energy condition. Mathematically, we can write $Q_{\rm j} = \frac{4PV}{t_{\rm activ}}$, where P and $t_{\rm activ}$ are lobe pressure and the duration of active phase of the jets respectively at the minimum energy condition. V is the lobe volume. To determine the spectral ages and hence $t_{\rm activ}$, we have fitted Jaffe-Perola models (Jaffe & Perola 1973) to the radio spectra of all the sources. We used the formalism of Konar et al. (2008) to estimate the minimum energy magnetic field ($B_{\rm min}$), and hence to estimate the total pressure P ($= \frac{1}{3}(\epsilon_{\rm B,min} + \epsilon_{\rm e,min})$) of the lobes, which we take to be cylinders for the purposes of estimating volume. The method of estimating spectral age is described in detail by Konar et al. (2012, 2013). The method of estimating $Q_{\rm j}$ that we adopt neglects the work done on the external environment due to driving shocks into the external medium. However, as numerical modelling in realistic environments (Hardcastle & Krause 2013) shows that the work done on the external medium is comparable to the internal energy of the lobes over the greater part of the lifetime of the RG, we expect this to give at worst a systematic underestimate of $Q_{\rm j}$, which would not affect any observed correlation between $Q_{\rm j}$ and $\alpha_{\rm inj}$.

3.3 Correlations

In this section we discuss the results related to $\alpha_{\rm inj}$ and $Q_{\rm j}$ for our sample. We begin by plotting $\alpha_{\rm inj}$ for the outer doubles against that of the inner doubles. This plot shows a correlation (see top panel of Fig. 2), significant at the 95 per cent level on a Spearman rank test, indicating that $\alpha_{\rm inj}$ is quite similar in the two different episodes of jet activity of most of the DDRGs in our sample. We discuss this remarkable result below.

We also attempted to find any possible correlation between $\alpha_{\rm inj}$ and $Q_{\rm j}$ of FR II radio galaxies. We compiled a small sample of Large Radio Galaxies (LRGs) which have well constrained spectra, and good estimation of $\alpha_{\rm inj}$ and spectral ages published by Jamrozy et al. (2008) and Nandi et al. (2010). From the spectra and ages, we estimated $Q_{\rm j}$ for our sample of DDRGs and LRGs (see Table 2, online material), though we were unable to determine spectral ages for three of our DDRGs. The determination of spectral ages, and the estimation of $\alpha_{\rm inj}$ and $Q_{\rm j}$, were carried out in the same way for

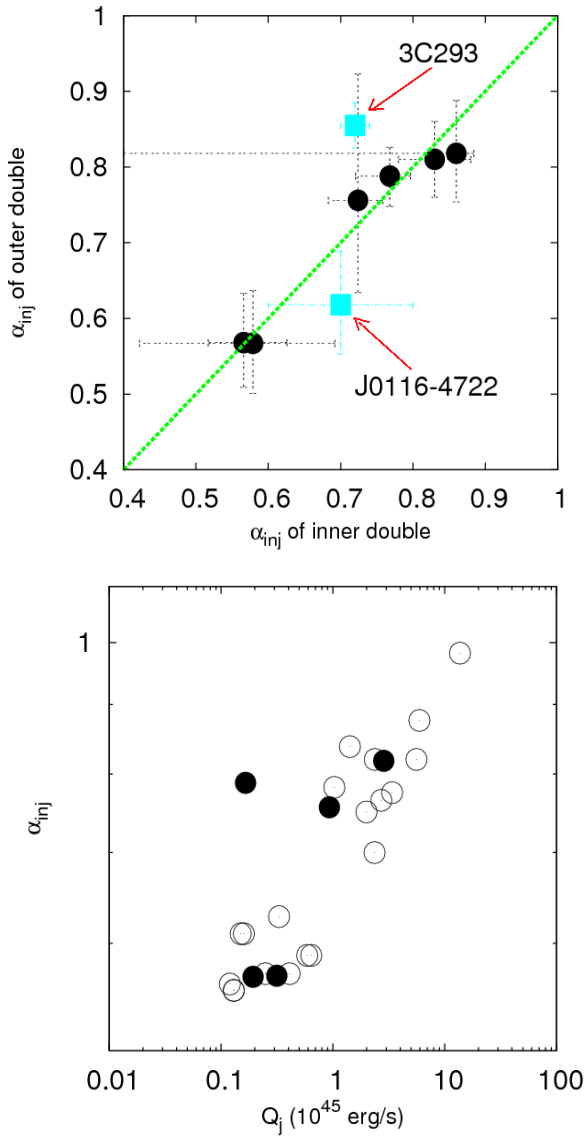

Figure 2. Top panel: $\alpha_{\rm inj}$ for the outer and inner doubles of our sample of DDRGs. Two objects, indicated by filled triangles, have slightly dissimilar values of $\alpha_{\rm inj}$ in the two episodes, but all the other sources lie close to the line of equality (dotted line). Bottom panel: $\alpha_{\rm inj}$ vs. $Q_{\rm j}$ plot for the FRII RGs considered in this paper. A filled circle represents an entire outer double of a DDRG. An open circle represents a single lobe of a LRG, except 3C46 and 3C452 which are plotted as entire doubles.

both samples. We plotted $\alpha_{\rm inj}$ vs. $Q_{\rm j}$ (see bottom panel of Fig. 2) and found a correlation which is significant at better than 99.9 per cent on a Spearman rank test.

To understand these results we need to consider the dynamics of radio galaxies, particularly in the double-double phase, and that is the topic of the following section of the paper.

4 RELATIVISTIC DYNAMICS OF RADIO GALAXIES

4.1 Introduction

Observationally it is clear that the formation of DDRG and Triple-Double Radio Galaxy (TDRG) morphologies is due to the episodic jet forming activity (see Konar et al. 2006, 2012, 2013). However, there are two plausible models to explain how the inner double morphology can be created. Those two models are the 'classical FR II model' and 'bow shock model' (see Konar et al. 2013). In the first of these, the inner lobes are formed in the same way as the Single-Double Radio Galaxies (SDRGs) and the outer doubles of DDRGs, i.e., by the back-flowing relativistic plasma injected at the hotspots. This is what is referrred to as 'classical FR II model'. In the 'bow shock model' the inner doubles are created by re-acceleration of the particles at the bow shocks driven into the outer cocoon material created by the almost ballistically moving jet heads (Brocksopp et al. 2007, 2011; Safouris et al. 2008). While some sources are indeed well described by the 'bow shock model', there is some morphological evidence that it does not apply to all DDRG (Safouris et al. 2008). In addition, crucially, there seems to be no real reason to expect a similar injection index in the inner and outer doubles in this model, as observed (Section 3.3) since the shocks in the hotspots of the outer doubles and the bow shock in the inner double should have very different properties. Although the bow shock model must be correct at some level (i.e. there must be some reacceleration of particles if the new lobe drives a shock through the old one) the observations of correlated injection indices suggest that emission from the bow shock cannot dominate the observed inner double[2]. In this paper we therefore concentrate on the 'classical FRII model'.

As discussed in more detail by Konar et al. (2013, Section 1), the main problem with the classical FRII model for the inner doubles is, or is perceived to be, the very rapid hotspot advance speed expected due to the low density in the outer lobes. The presence of compact components at the jet heads of the inner doubles of all FR II DDRGs, together with the observation that the inner doubles can extend back for significant distances towards the core, motivates the idea that there is entrainment/ingestion of matter from the thermal ambient medium into the large-scale lobes, increasing the internal density of these lobes and hence reducing the hotspot advance speed. Kaiser, Schoenmakers & Röttgering (2000) have argued that the Kelvin-Helmholtz and Raleigh-Taylor instabilities do not grow quickly in the contact discontinuity separating the magnetized ralativistic plasma of the radio lobes and the thermal ambient medium. According to them, the time scales ($\sim 10^8$ yr) of those instabilities on the relevant scale length (~ 1 kpc) are higher than the age of the outer doubles of most of the known DDRGs. Kaiser et al. (2000) argued that the thermal matter entrainment into the radio lobes is therefore a slow and inefficient process. They proposed a model in which the thermal matter is ingested into the cocoon (or lobes) in the following way. When the jets propagate through the thermal ambient medium, the jet-heads drives shocks into that ambient medium, which is a two phase medium with cooler and denser clumps embedded in the hot gaseous Inter-Galactic Medium (IGM). Since the clumps are heavier, they are not imparted sufficient momentum by the passage of the bow shock. As a result, the contact discontinuity overtakes those shocked clumps which ends up being inside the cocoon, or the lobes. These clouds then dif-

[2] It is worth noting one special case: if the shock driven into the outer lobe is quite weak, so that there is little particle acceleration and instead simply adiabatic compression of the particles and field, then the compressed material would indeed be expected to have the same injection index as the outer lobe, since the inner double would simply be rejuvenated outer lobe material. This model may be applicable in some weak sources on galactic scales (see Mingo et al. 2012) but the other properties of the inner doubles do not seem consistent with weak shocks, so we do not consider it further here.

fuse inside the cocoon throughout the cocoon volume, and finally mix with the cocoon matter. This increases the mass density inside the cocoon and provides a favourable situation for the inner double to form hotspots and well-confined inner lobes. The main problem with this model is the lack of any strong observational evidence that there is a significant density of thermal matter in the lobes: this should be the case for all large FRIIs, and so will be readily testable in coming years with low-frequency polarization observations. In the meantime, we shall explore the consequences of alternative models, in which we assume that the FR II lobes contain only nonthermal pair plasma.

4.2 Comparison of the dynamics of lobe protons, if at all present, with that of lobe electrons

Whether the jet matter consists of electron-proton (hereafre e^-p^+) or electron-positron (hereafter e^-e^+) plasma is so far a debatable issue. However, if the jet matter does consist of e^-p^+ plasma, we would like to assess the possible dynamical consequences of the additional heavy particles.

The results of Croston et al (2005) suggest that the mean kinetic energy of lobe protons can be at most similar to the mean kinetic energy of lobe electrons. So we can write

$$\langle(\gamma_p - 1)m_pc^2\rangle < \langle(\gamma_e - 1)m_ec^2\rangle$$

where γ_p and γ_e are the Lorentz factors of a proton and an electron respectively, m_p and m_e are the masses of a proton and an electron respectively and c is the speed of light. The angular brackets represent the mean of a quantity. After simplifying the above relation we get

$$\langle\gamma_p\rangle < 1 + (\langle\gamma_e\rangle - 1)\left(\frac{m_e}{m_p}\right) \quad (1)$$

The mean Lorentz factor of the radiating particles in a radio lobe can be given by

$$\langle\gamma_e\rangle = \frac{\int \gamma_e N(\gamma_e) d\gamma_e}{\int N(\gamma_e) d\gamma_e}.$$

Assuming a power law distribution of radiating electrons, $N(\gamma_e) = N_0\gamma_e^{-\delta}$ ($\delta > 2$) and integrating from γ_1 to γ_2, we obtain

$$\langle\gamma_e\rangle = \frac{\delta - 1}{\delta - 2}\frac{\gamma_1^{2-\delta} - \gamma_2^{2-\delta}}{\gamma_1^{1-\delta} - \gamma_2^{1-\delta}} \quad (2)$$

For FR II radio lobes the electrons have Lorentz factors from 10 to $> 10^5$ with a typical power law index of 2.5. For our representative estimate we assume that $\gamma_1 = 10$, $\gamma_2 \to \infty$ and $\frac{m_e}{m_p} = \frac{1}{1836}$. This yields $\langle\gamma_e\rangle \sim 30$. If we estimate the average value of $\langle\gamma_p\rangle$ from equation (1) of such typical FR II lobes, we obtain

$$1 \lesssim \langle\gamma_p\rangle < 1.0158 \quad (3)$$

(as Lorent factor cannot be lower than 1). A Lorentz factor of 1.0158 corresponds to a speed of $0.1757c$, which is mildly relativistic. We may define an effective temperature ($T_p^{\rm L}$) for the lobe protons such that

$$k_BT_p^{\rm L} = (\langle\gamma_p\rangle - 1)m_pc^2, \quad (4)$$

where k_B is the Boltzmann constant. This gives an average effective temperature $T_p^{\rm L} < 1.72 \times 10^{11}$ K, which is similar to the nonthermal temperature (see equations (13) and (14) for definition) of radiating particles. This simply means that the protons, if at all fed by the FR II jets, have not been accelerated in the JTS as efficiently as the electrons. In the relativistic DSA model, the flattest value of $\alpha_{\rm inj} \sim 0.62$ (Kirk et al. 2000). For $\alpha_{\rm inj} \sim 0.62$, we will get the maximum possible value of $\langle\gamma_e\rangle$, $\langle\gamma_p\rangle$ and $T_p^{\rm L}$. Those values are $\langle\gamma_e\rangle = 51.67$, $\langle\gamma_p\rangle < 1.0276$ and $T_p^{\rm L} < 3.01 \times 10^{11}$ K.

Since we have an estimate of $\langle\gamma_e\rangle$, we can estimate the number density of radiating particles in the radio lobes in the following way. The radiating particles are in energy equipartition with the magnetic field, so we can write

$$(\langle\gamma_e\rangle - 1)n_em_ec^2 = \frac{B_{\rm eq}^2}{8\pi},$$

where $B_{\rm eq}$ is the equipartition magnetic field strength. From this we get an expression for the number density of electrons in the lobes:

$$n_e = \frac{1}{(\langle\gamma_e\rangle - 1)m_ec^2}\frac{B_{\rm eq}^2}{8\pi}. \quad (5)$$

For $B_{\rm eq} = 5$ μG, $\gamma_1 = 10$ and $\gamma_2 \to \infty$ limit, which are typical for the outer lobes of DDRGs, equations (2) and (5) yield

$$n_e \sim 7 \times 10^{-8}{\rm cm}^{-3}$$

for $\alpha_{\rm inj} = 0.62$ (flattest possible value) and

$$n_e \sim 4 \times 10^{-8}{\rm cm}^{-3}$$

for $\alpha_{\rm inj} = 0.75$ (a typical value). Thus, if the jets are e^-p^+, an equal number of protons in the outer lobe plasma would be more than enough to allow hotspot formation in the inner jet head and confinement of the inner lobes, a point that we shall return to in Section 4.5.4. (However, we shall also show that hotspot formation and inner lobe confinement are possible even for a pure e^-e^+ plasma in the outer cocoon.)

As a summary of this section, we can write

$$\langle E_p^{\rm kin}\rangle < \langle E_e^{\rm kin}\rangle, \quad (6)$$

and

$$1 \lesssim \langle\gamma_p\rangle < 1.0276, \quad (7)$$

These place very good constraints on the proton acceleration at the JTS, if at all protons exist in the jet material. In the next section we show that this implies that it is highly likely that the jet composition is e^-e^+.

4.3 Composition of FR II jets

Here we argue that e^-e^+ jets are more viable than e^-p^+ jets, at least in FR II radio galaxies. If the FR II jets are made of e^-p^+, then in the jet flow electrons and protons must travel together with the bulk Lorentz factor, $\Gamma_{\rm j}$ of the jet to avoid charge separation. The constancy of spectral indices in two episodes of DDRGs demands that the $\Gamma_{\rm j}$ be > 10 (see Section 5.2), so that the JTS can be considered to be a strong shock. Therefore, even if the protons collectively behave as a (probably collisionless) background fluid in which the electrons are embedded as test particles, a significant amount of the bulk kinetic energy of the upstream flow is expected to be converted into the internal energy of the proton fluid. Since the JTS is a strong relativistic shock, the average value of the kinetic energy of the protons would be expected to be *higher* than that of the leptons in the lobes. As Drury (1983) suggests, "The abundances of a species in the high energy particles relative to that in the (upstream) plasma should be a smooth and probably increasing function of its mass to charge ratio". This is the so-called 'selectivity of injection' of the particles, though there exists no quantitative

theory for it. Effectively, protons in the upstream jet fluids will be more easily injected into the shock to participate in the DSA than the electrons: this will give rise to a larger number of accelerated protons than leptons in the lobes. Though Drury advanced the concept of 'selectivity of injection' in the context of non-relativistic DSA, there is no physically plausible reason why this 'selectivity of injection' should not be qualititatively valid for relativistic DSA as well. However, as shown in the previous subsection, the results of Croston et al. (2005) indicate that the protons are energetically not dominant, and thus cannot be accelerated to higher energies than electrons. Hence, if our assumptions hold, jets must be composed of e^-e^+ rather than e^-p^+. We will consider the jet plasma to be e^-e^+ in what follows.

We note that work on FR I radio galaxies (e.g. McNamara & Nulsen, 2012) suggests that there are protons inside the FR I lobes. Recent observational results suggest that this is most probably due to the entrainment of thermal matter through the FR I jets (Croston et al. 2008), while there are various lines of evidence (e.g. Dunn, Fabian & Celotti 2006) that FR I jets are electron-positron at their bases. We would argue therefore that jets are originally e^-e^+ for both FR I and FR II sources. Entrainment both slows down the FR I jets and causes their lobes to have a non-negligible proton content. FR II jets are not so strongly affected by entrainment (Bicknell 1995) and their lobes should thus be mainly filled with e^-e^+ plasma, consistent with observations (e.g. Croston et al. 2004) that show that pressure balance can be achieved in the lobes with only e^-e^+ together with magnetic fields whose strengths are derived from inverse-Compton observations. Since our DDRGs are all FR IIs, we will consider both jet and lobe plasma to be e^-e^+ in what follows.

4.4 Momentum balance at the jet heads

Considering the conservation of momentum flow across the JTS and the bow shock allows us to find the hotspot velocity with respect to the host galaxy frame. Fig. 3[3] shows the schematic diagram of a jet head. Here we discuss the momentum balance at the hotspot, balancing the momentum flux coming up the jet with the ram pressure at the front of the lobe as it is driven through the ambient medium. The momentum balance equation can be written as (see equation (A15) in Appendix)

$$\beta_{\rm hs} = \frac{1}{1+\eta}\beta_{\rm j}, \tag{8}$$

where $\beta_{\rm hs}$ and $\beta_{\rm j}$ are the hotspot velocity and jet bulk velocity in the host galaxy frame, and

$$\eta = \sqrt{\frac{\beta_{\rm j} c A_{\rm h}}{Q_{\rm j}} w_{\rm a}} \tag{9}$$

(from equation A16), where $A_{\rm h}$ is the area over which the jet momentum flux is distributed, c is the speed of light, $Q_{\rm j}$ is the jet power as measured in the host galaxy frame and $w_{\rm a}$ is the relativistic enthalpy density of the ambient medium surrounding the jet and lobes. The proper speed of the hotspot in the host galaxy

[3] **For simplicity we neglect the existence of multiple hotspots in this discussion, but that their existence implies that sometimes the deceleration (Gopal-Krishna & Wiita 1990) and particle acceleration (Hardcastle, Croston & Kraft 2007) may be distributed over a larger region than would be expected in a simple planar shock model. However, this makes no difference to our argument.**

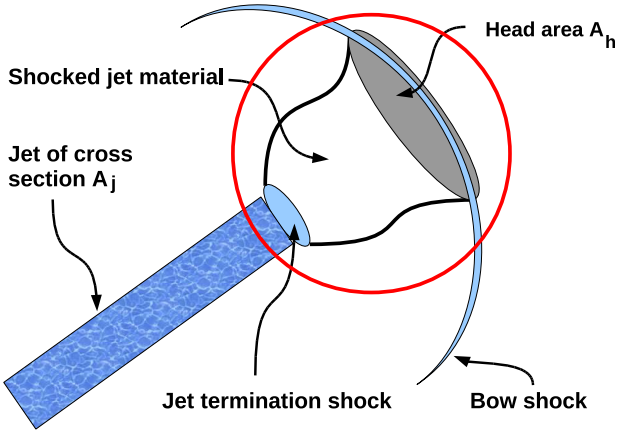

Figure 3. A schematic diagram of a hotspot-complex (encircled by the red cicle) at the head of an FR II jet.

frame, $u_{\rm hs}$, and that of the jet matter in the hotspot frame, $u_{\rm j,hs}$ are relevant to the discussion of the formation of the JTS and particle acceleration there. These speeds are given by

$$u_{\rm hs} = \frac{\beta_{\rm hs}}{\sqrt{1-\beta_{\rm hs}^2}} \tag{10}$$

$$u_{\rm j,hs} = \Gamma_{\rm j,hs}\beta_{\rm j,hs} = \Gamma_{\rm j}\Gamma_{\rm hs}(\beta_{\rm j} - \beta_{\rm hs}) \tag{11}$$

In this formulation we can create the most general expression for the ambient medium and, depending upon the situation, we can use the values of the different parameters to distinguish between a thermal and nonthermal ambient medium. In the outer lobes of DDRGs there can be in general nonthermal particles (e^-e^+) together with a (presumably small) amount of ingested thermal particles (e^-p^+). Similarly, in the thermal ambient medium of a radio galaxy there can be in general thermal and nonthermal particles. However, we know that the thermal particles in FR II radio lobes (Croston et al. 2005) and the nonthermal particles in thermal ambient medium of radio galaxies are not energetically dominant. We assume therefore that the jet and lobe are composed of e^-e^+ plasma.

Therefore, the most general expression for $w_{\rm a}$, which contain both thermal and nonthermal components, can be written as

$$w_{\rm a} = \text{rest mass energy} + \text{remaining internal energy} + \text{pressure}$$

$$w_{\rm a} = \left[n_p m_p c^2 + n_e m_e c^2\right] + \left[\frac{3}{2}n_p^{th}k_B T_p^{th} + \frac{3}{2}n_e^{th}k_B T_e^{th} + \{(\epsilon_e^{nt} + \frac{B_{\rm a}^2}{8\pi})\}\right] + \left[n_p^{th}k_B T_p^{th} + n_e^{th}k_B T_e^{th} + \{\frac{1}{3}(\epsilon_e^{nt} + \frac{B_{\rm a}^2}{8\pi})\}\right] \tag{12}$$

where $n_p = n_p^{th}$ is the number density of the thermal protrons only (and no nonthermal protons), $n_e = n_e^{th} + n_e^{nt}$ is the total number density of leptons (thermal + nonthermal), $\epsilon^{th} = \frac{3}{2}n^{th}k_B T^{th}$ is the kinetic energy density of the thermal particles, $P^{th} = n^{th}k_B T^{th}$ is the partial pressure of the thermal partilcles, ϵ_e^{nt} is the energy density of the nonthermal electrons, and $B_{\rm a}$ is the magnetic field strength in a general ambient medium.

For nonthermal electrons which are ultrarelativistic, we define nonthermal electron temperatures (this is not a thermodynamic

temperature) such that they follow

$$P_e^{nt} = n_e^{nt} k_B T_e^{nt}, \tag{13}$$

and

$$\epsilon_e^{nt} = \frac{1}{\gamma - 1} P_e^{nt} = 3 n_e^{nt} k_B T_e^{nt}, \tag{14}$$

where $\gamma = \frac{4}{3}$ is the adiabatic index of the gas consisting of those relativistic particles. Equations 13 and 14 satisfy the relations $P = \frac{1}{3}\epsilon$. For thermal gas $\gamma = \frac{5}{3}$, for a nonthermal distribution of ultrarelativistic particles $\gamma = \frac{4}{3}$. If the nonthermal particles are nonrelativistic or mildly relativistic then we cannot characterise the gas by any constant adiabatic index. However, since the particles are sufficiently scattered by the irregualrities of the magnetic fields, we expect that such a gas is likely to have an adiabatic index in the range $\frac{4}{3} < \gamma < \frac{5}{3}$.

For the SDRGs and the outer doubles of the DDRGs the ambient medium is the thermal gas around the radio galaxy. This means that $n_p^{nt} = n_e^{nt} = 0$ (so $\epsilon_p^{nt} = 0$, $\epsilon_e^{nt} = 0$) and $B_a = 0$ are good approximations. An expression for the enthalpy density, as obtained from the equation (12), is

$$w_{\rm a}^{th} = \left[n_p^{th} m_p c^2 + n_e^{th} m_e c^2 + \frac{5}{2} n_p^{th} k_B T_p^{th} + \frac{5}{2} n_e^{th} k_B T_e^{th} \right]$$

$$= \left[n_p^{th} m_p c^2 + n_e^{th} m_e c^2 + \frac{5}{2} (n_p^{th} + n_e^{th}) k_B T^{th} \right]. \tag{15}$$

Here we have substituted $T_p^{th} = T_e^{th} = T^{th}$, as electrons and protons are usually in thermal equilibrium with each other in the thermal environment of SDRGs.

For the inner doubles of double-double radio galaxies, the ambient medium is the cocoon matter of the outer double and is dominated by nonthermal matter. There might or might not be cold matter in the outer cocoon of the DDRGs, but in the light of the observational results of Croston et al. (2004, 2005), and as discussed above, there is no evidence for significant thermal matter inside the radio lobes. For the outer cocoon, we therefore assume that $n_p^{th} \sim 0$ and $n_e^{th} \sim 0$. The expression for the enthalpy density, as obtained from equation (12), is then

$$w_{\rm a}^{nt} = n_e^{nt} m_e c^2 + \frac{4}{3} (\epsilon_e^{nt} + \frac{B_{\rm a}^2}{8\pi}). \tag{16}$$

4.5 Relativistic jet dynamics

It is the jet dynamics which control the hotspot speed, and therefore the strength of the JTS and bow shock. From our momentum balance analysis (Section 4.4), we know that the nature of the ambient medium is crucial in determining many aspects of jet dynamics. However, the ambient media for the inner jets and the outer jets of a DDRG are quite different. The outer jets and lobes propagate through a comparatively dense thermal medium, whereas, the inner jets and lobes propagate through a very tenuous non-thermal medium. We will discuss the effect of such differing ambient media on the jet dynamics in what follows.

4.5.1 Variation of hotspot speed with various parameters

From equation (8), we know that the hotspot speed depends on the parameter η which itself is a function of various other parameters, such as $\beta_{\rm j}$, $A_{\rm h}$, $w_{\rm a}$ and $Q_{\rm j}$. In this subsection we show graphically how the proper speeds of hotspot motion measured in the host galaxy frame ($u_{\rm h}$) and the bulk jet motion measured in the hotspot frame ($u_{\rm j,hs}$) change with the number density of particles (protons) of the ambient medium, with $\Gamma_{\rm j}$, $B_{\rm a}$, $r_{\rm h}$ and $Q_{\rm j}$ being treated as parameters.

In Fig. 4, $u_{\rm h}$ vs. $n_{\rm a}^{th}$ and $u_{\rm j,hs}$ vs. $n_{\rm a}^{th}$ curves are shown for two different values of $B_{\rm a}$ in the left panel. A zoomed portion of the left panel is shown in the right panel. For both panels we have assumed a jet Lorentz factor $\Gamma_{\rm j} = 5$ (as measured in the host glaxy frame), a temperature of the thermal particles of the ambient medium $T_{\rm a}^{\rm th} = 3 \times 10^7$ K, a jet head radius, $r_{\rm h} = 5$ kpc, and a jet power, $Q_{\rm j} = 10^{44}$ erg s^{-1}. The thick continuous red curves are for the variation of $u_{\rm h}$ and $u_{\rm j,hs}$ of the jets propagating through an ambient medium which has neither magnetic field nor nonthermal particles; hereafter we refer to this sort of ambient medium as a 'pure thermal ambient medium', and it is a good approximation for the medium surrounding the outer double of a DDRG or any SDRG. The thin green dashed curves are for the variation of $u_{\rm h}$ and $u_{\rm j,hs}$ of the jets propagating through an ambient medium with thermal matter, constant magnetic field $B_{\rm a}$ =5 μG, nonthermal radiating electrons in energy equipartition with the magnetic field (and no nonthermal (jet-fed) protons). Hereafter, we refer to this sort of ambient medium as an 'impure ambient medium'. In the impure ambient medium the number density of nonthermal electrons does not matter as their rest mass energy is negligible compared to their kinetic energy and the rest mass energy of the thermal protons. A third kind of ambient medium contains only nonthermal particles (electrons and positrons) and magnetic field, but no thermal matter; we can refer to this kind of ambient medium as a 'pure nonthermal ambient medium'. Though the thin green curves are for an impure ambient medium, as we go towards very low particle density, e.g. $n_p^{th} < 10^{-8}$ for the case in Fig. 4, the nonthermal energy (nonthermal particle energy + magnetic field energy) starts dominating the thermal energy, and for even lower values of n^{th} an impure ambient medium becomes equivalent to a pure nonthermal ambient medium, which is perhaps the case for the inner doubles of DDRGs.

4.5.2 Propagation of jets through impure ambient media: the case of inner doubles

In Fig. 5, $u_{\rm h}$ vs. n_p^{th} and $u_{\rm jh}$ vs. n_p^{th} curves are shown for two different values of jet head radius, $r_{\rm h}$ in each panel. In this study we have assumed an impure ambient medium with $B_{\rm a} = 5$ μG, $T_{\rm a}^{th} = 3 \times 10^7$ K. We have also fixed the jet power to $Q_{\rm j} = 10^{44}$ erg s^{-1}. The smaller the jet head radius, the faster the jet head (or hotspot) can move through a given ambient medium, provided all other parameters are held constant. This is quite natural and conforms with our common sense that a thinner object can penetrate easily through any given medium. The faster the speed of the hotspot, the slower is the jet bulk speed, as observed from the hotspot frame. Fig. 5 shows the variation $u_{\rm h}$ (and $u_{\rm jh}$) vs. n_p^{th} curves for two different values of $\Gamma_{\rm j}$. Keeping all other parameters fixed, if $\Gamma_{\rm j}$ decreases from 5 to 1.2 then the entire curves showing the variations of $u_{\rm jh}$ are displaced downwards. The jet Lorentz factor thus has an important role in creating the JTS as well as the bow shock around the jet head (see Section 4.5.4 for detail).

4.5.3 Various plasma waves in the nonthermal cocoon plasma

In a magnetized plasma, disturbances can propagate via either pure sound waves (parallel to the field lines) and three kinds of magnetosonic waves. Those magnetosonic waves are fast magnetosonic

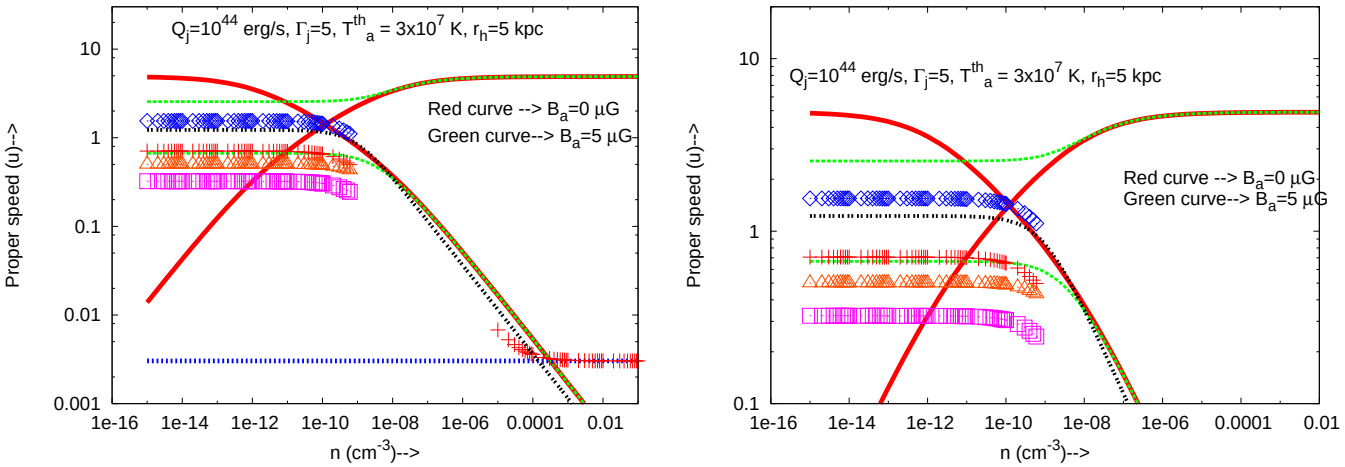

Figure 4. Left panel: the variation of proper speed of the hotspot motion ($u_{\rm h}$) as measured in the host galaxy frame and the upstream jet bulk motion as measured in the hotspot frame ($u_{\rm j,hs} = \Gamma_{\rm jh}\beta_{\rm jh}$) as a function of the number density (n_p^{th}) of thermal particles (protons) in the ambient medium. The thick red curves show the variation of $u_{\rm h}$ and $u_{\rm j,hs}$ with n_p^{th} in a 'pure thermal ambient medium'. The thin dashed green curves show the variations of $u_{\rm h}$ and $u_{\rm jh}$ for an 'impure ambient medium' with constant magnetic field, $B_{\rm a}$ =5 μG and no jet-fed protons. Among the red and green curves, the ones which are rising as n_p^{th} decreases are showing the variation of $u_{\rm h}$, and the others are showing the variation of $u_{\rm j,hs}$. Equipartition between electron and field energy has been assumed. For all the curves a jet head radius $r_{\rm h} = 5$ kpc, jet Lorentz factor $\Gamma_{\rm j} = 5$, ambient medium thermal temperature $T_{\rm a} = 3 \times 10^7$ K, and jet power $Q_{\rm j} = 10^{44}$ erg s^{-1} have been used in the calculations. The black double-dotted curve shows the variation of the Alfven speed. The blue dotted horizontal line in the left panel is the sound speed in a 'pure thermal ambient medium'. The other symbols indicates the variation of the magnetosonic wave mainly in the 'pure nonthermal ambient medium'. Those are as follows. Blue diamonds: the speed of the fast magnetosonic wave; orange triangles: the speed of the intermediate magnetosonic wave (or shear Alfven wave); and pink squares: the slow magnetosonic wave. Red plus (+): the sound speed in the absence of magnetic field. Note that we have drawn the sound speed only in the ultrarelativistic and nonrelativistic regime, as there is no simple method of calculating the appropriate adiabatic index in between these two regimes. Right panel: a zoomed-in version of a portion of the same plot.

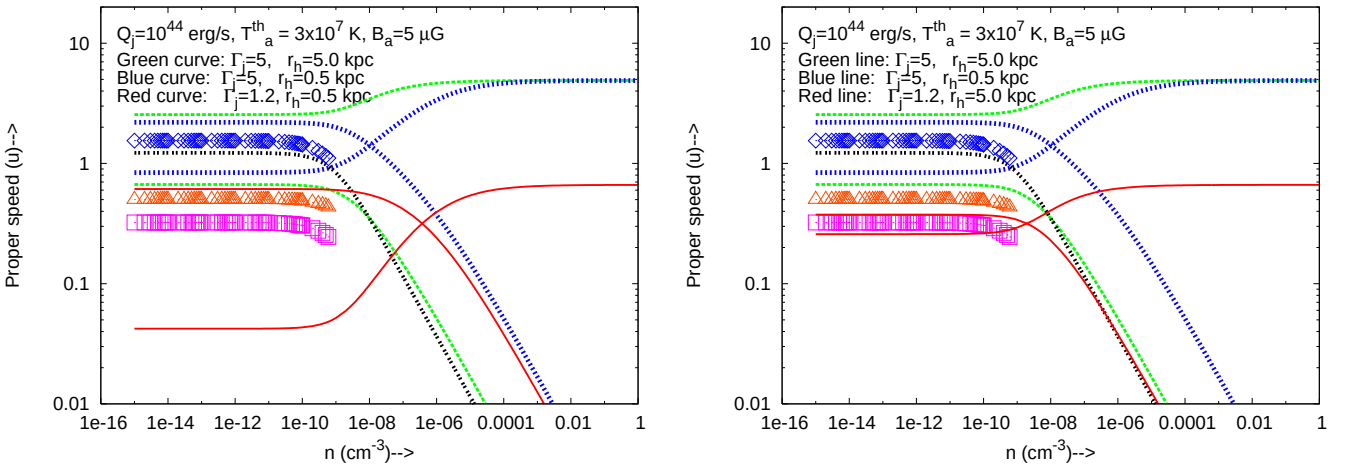

Figure 5. The variation of proper speed of the hotspot motion ($u_{\rm h}$) as measured in the host galaxy frame and the upstream jet bulk motion as measured in the hotspot frame ($u_{\rm j,hs} = \Gamma_{\rm j,hs}\beta_{\rm j,hs}$) as a function of the number density (n_p^{th}) of thermal particles in the ambient medium. All the curves are for $Q_{\rm j} = 10^{44}$ erg s^{-1}, $T_{\rm a}^{th} = 3 \times 10^7$ K, $B_{\rm a} = 5$ μG. The curves that fall and saturate as n_p^{th} decreases show the variation of $u_{\rm j,hs}$ with $n^{\rm th}$. The curves that rise (except the double-dotted black curve) as n_p^{th} decreases show the variation of $u_{\rm h}$. The green and blue curves are for $\Gamma_{\rm j} = 5$ and the red curves are for $\Gamma_{\rm j} = 1.2$. The rest of the symbols have the same meaning as in Fig. 4. The green curves are for $r_{\rm h} = 5$ kpc. The blue curves are for $r_{\rm h} = 0.5$ kpc. The red curves on the left panel have $r_{\rm h} = 0.5$ kpc, and on the right panel have $r_{\rm h} = 5$ kpc. For simplicity, the variation of the speed of pure sound waves is omitted in this plot.

wave (herefter, fast wave) Intermediate wave (or shear Alfvén wave) and slow magnetosonic wave (hereafter, slow wave). For the general case of relativistic plasma with anisotropic pressure (the pressure parallel and perpendicular to field lines are different), the dispersion relations for magnetosonic waves have been worked out by Gedalin (1993). However, we know that the radio jets and lobes are moving either through a nonrelativistic thermal plasma (for outer doubles of DDRG or SDRGs), or through an ultrarelativistic magnetized nonthermal plasma (for inner doubles of DDRGs). We have already referred to these as a 'pure thermal ambient medium' and a 'pure nonthermal ambient medium' respectively. The adiabatic Equation of State (EoS) of both kinds of plasma can be written with a polytropic index, $\gamma_{\rm ad}$, as

$$P \propto \rho^{\gamma_{\rm ad}}, \qquad (17)$$

where $\gamma_{\rm ad} = \frac{5}{3}$ for pure thermal ambient medium and $\gamma_{\rm ad} = \frac{4}{3}$ for pure nonthermal ambient medium. This polytropic EoS can be used for our purpose. A point to note here is that even if the plasma is mildly to moderately relativistic, i.e., between nonrelativistic and ultrarelativistic limits, the adiabatic EoS of the plasma can be still treated as a monatomic polytropic gas with $\frac{4}{3} < \gamma_{\rm ad} < \frac{5}{3}$ (Synge 1957; Anile 1989). However, the problem is that in the case of a strong relativistic shock, the adiabatic index in the downstream may be different from that of the upstream flow. In our specific case, though, we have enough evidence, as already discussed, that the cocoon gas in outer doubles of FR II DDRGs (or in general FR II lobes) can be treated as an ultrarelativistic gas. Therefore an adiabatic EoS with a polytropic index of $\frac{4}{3}$ can well describe the adiabatic behaviour of the relativistic plasma in FR II lobes. Even if there are some thermal/nonthermal protons in the radio lobes, we have shown in equation (6) that the kinetic energy in protons is much less than that in the radiating electrons. This means that most of the pressure is contributed by the radiating particles and magnetic field in FR II radio lobes. Since the radiating particles are ultrarelativistic, an adiabatic EoS with a polytropic index $\gamma_{\rm ad} = \frac{4}{3}$ is guaranteed. If jet-fed protons and ingested thermal matter exist in cocoon matter, they can only contribute to the mass density of the plasma. As far as the lobe plasma is concerned, we know that observations show that magnetic fields are not completely ordered (i.e. the degree of polarization observed in lobes is well below the maximal possible value) and so for simplicity, we will assume that the magnetic field lines are completely tangled, which means that the pressure of such a magnetoplasma is isotropic.

The EoS of the FR II jet matter is not known, but fortunately we do not need to know it, as the EoS of upstream fluid is immaterial for a strong relativistic shock. Since we know that JTS, at least in the large-scale lobes, are associated with efficient localized particle acceleration, it is reasonable to assume that all JTS are strong shocks.

Chou & Hau (2004) give a description of relativistic anisotropic MHD for a gyrotropic ultrarelativistic plasma. Their work is directly relevant for our case as they derived the dispersion relations for a gyrotropic plasma rather than a general plasma, as given e.g. by Gedalin (1993). The expressions for phase velocities of magnetosonic waves, from Chou & Hau (2004), reduce to the standard ones for a non-relativistic, isotropic and polytropic plasma. Since the cocoon plasma is very likely to exert isotropic pressure, we consider only the isotropic case from Chou & Hau (2004). Below we present the expressions of the speeds of various waves in a 'nonthermal cocoon plasma' whose pressure is dominated by nonthermal radiating particles.

The Alfvén wave speed is given by

$$V_A^2 = \frac{\frac{B^2}{4\pi}}{\rho^0 c^2 + (\epsilon^{nt} + P^{nt} + \frac{B^2}{4\pi})} c^2 \qquad (18)$$

and the pure sound wave speed in the absence of a magnetic field is given by

$$V_{\rm son}^2 = \frac{\gamma_{ad} P^{nt}}{\rho^0 c^2 + (\epsilon^{nt} + P^{nt})} c^2 \qquad (19)$$

(Chou & Hau, 2004). The phase speed of the intermediate wave is given by (Chou & Hau 2004)

$$V_I^2 = \frac{\frac{B^2}{4\pi}\cos^2\theta}{\rho^0 c^2 + (\epsilon^{nt} + P^{nt} + \frac{B^2}{4\pi})}, \qquad (20)$$

and the phase speed of the fast and slow wave mode can be given by

$$V_{\rm f,s}^2 = \frac{1}{2}(b^{'} \pm \sqrt{b^{'2} - 4C'}), \qquad (21)$$

where $b^{'} = b_{\rm is}/a_{\rm is}$ and $C^{'} = C_{\rm is}/a_{\rm is}$; these constants are described in Appendix B. For estimating numerical values for the plots in Fig. 4 and 5, we have used $\langle\cos^2\theta\rangle = \frac{1}{3}$.

We have used the equations (18)-(21) to calculate the speed of sound, Alfven and magnetosonic waves of the realistic nonthermal plasma of the outer cocoon of a hypothetical DDRG for our study and to generate the plots in Fig. 4 and 5. On the other hand, we have used equation (10) and (11) to estimate $u_{\rm hs}$ and $u_{\rm j,hs}$ respectively. Energy equipartition between radiating particles and magnetic field has been used; inverse-Compton observations show that this is a good approximation (Croston et al. 2005), as far as the FR II lobes are concerned.

4.5.4 *Creation of jet termination shock and bow shock in the inner double*

Any FR II jet can, in principle, create two shocks. One is the JTS, which is due to the sudden slow down of the jet flow when the jet flow encounters the slow-moving downstream lobe material. The other is the bow shock in the ambient medium around the front of the lobe. In other works, the JTS develops in the jet/lobe matter itself, whereas the bow shock develops in the ambient medium through which the lobe ploughs its way. Since both the jet matter as well as the nonthermal ambient medium of the inner jets of a DDRG are relativistic magnetoplasma, we must compare the speed of the bulk motions with the speeds of magnetosonic waves rather than just sound waves. In any magnetoplasma a pure sound wave without magnetic field disturbance can exist only for propagation parallel to the field lines. The magnetic field energy density is comparable to the kinetic energy density of the particles, hence the magnetic field and its energy density cannot be neglected. Given that the magnetic field is largely tangled, no pure sound wave without magnetic field disturbance exists in the radio lobe plasma. In any magnetised plasma there exist 3 magnetosonic waves as discussed in the previous section. Therefore, there exist three types of shocks, corresponding to bulk flows exceeding the speed of each of the magnetosonic waves. The jet matter has a speed close to the speed of light in the host galaxy frame. However, the strength of the JTS depends on the speed of the jet matter with respect to the hotspot frame, which is determined by the ram pressure balance equation given in equation (8). As long as the ambient medium can provide enough ram pressure so that the bulk speed of the upstream jet matter in the hotspot frame is faster than at least the slow magnetosonic wave, a JTS will form at the jet head in both inner and outer doubles of any DDRG during their active phase. Our objective in this section of the paper is to investigate whether this is indeed the case even when the inner jets propagate through an extremely tenuous outer-cocoon plasma containing no significant ingested thermal plasma.

We show the variation of the proper speeds of hotspots ($u_{\rm hs}$) in the host galaxy frame and the upstream jet bulk motion ($u_{\rm j,hs}$) in the hotspot frame in Fig. (4) and (5), as usual assuming a jet power of $Q_{\rm j} = 10^{44}$ erg s^{-1}. Let us consider the thick red curves in Fig. (4). These curves are for $u_{\rm j,hs}$ and $u_{\rm hs}$ (see the figure caption) propagating through a pure thermal medium with no magnetic field, as is the case for the outer double of a DDRG. A jet Lorentz factor $\Gamma_{\rm j} = 5$ and a jet head radius $r_{\rm h} = 5$ kpc have been used to derive

the red curves. The sound speed of such a medium, given by

$$c_s = \sqrt{\frac{(5/3)k_B T^{th}}{\mu m_p}} \quad (22)$$

is constant with density and is shown by a blue horizontal line in the left panel of Fig. 4. We have assumed a poor cluster scale ambient medium of temperature $T^{th} = 3 \times 10^7$ K. We can clearly see that $u_{\rm hs}$ is much faster than the proper speed of sound in such an ambient medium. Therefore, the formation of a bow shock is inevitable for this case. However, the formation of JTS depends on the EoS of the jet material. For example, if the jet matter is ultrarelativistic plasma then JTS formation is possible only for a number density of protons in the ambient medium greater than $\sim 10^{-12}$ cm^{-3} as evident from Fig. 4; this condition is of course easily satisfied for all realistic environments. Similarly, if the jet matter is pure thermal (which is probably not the case) of temperature $T^{th} = 3 \times 10^7$ K, then the JTS will form up to a number density of protons of $\sim 10^{-16}$ cm^{-3} in the ambient medium.

When the same jet with same power and Lorentz factor propagates through a pure nonthermal tenuous plasma medium (which is possibly the case for the inner double of a DDRG) with cold protons (which contribute to only mass density and not to pressure), then the variation of $u_{\rm j,hs}$ and $u_{\rm hs}$ with the proton number density n_p of the ambient medium is shown by the green dashed curves in Fig. 4. We can see that for very low densities ($n_p \lesssim 10^{-8}$ cm^{-3}) of the ambient medium both a JTS and a bow shock can easily form. In this case, whatever may be the EoS of the jet material, the formation of JTS is inevitable, as $u_{\rm j,hs}$ is faster than even the fast wave for a relativistic EoS of the nonthermal plasma. We have studied this case for various jet-head radii and Lorentz factors in Fig. 5. As is evident from that Figure, if the jet matter has an ultrarelativistic EoS, then a jet with $\Gamma_{\rm j} = 1.2$ with both $r_{\rm h} = 5$ and 0.5 kpc cannot form JTS for $n_p \lesssim 10^{-10}$ cm^{-3}. The magnitude of this number is of interest because the number densities of radiating electrons in the outer lobes of FR II DDRGs are likely to be within the range $10^{-9} - 10^{-8}$ cm^{-3}. These plots show that, even without protons, JTS and bow shocks can form (generally doing so more easily for fast jets and large jet heads). However, if the lobe contains some protons (through either entrainment or ingestion), then the JTS is formed more easily. The key point from the results above is that thermal matter entrainment/ingestion into the outer lobes is not necessarily required to explain the confinement of inner lobes and the formation of JTS in the inner jets of DDRGs, although we do not rule out some amount of thermal matter ingestion into the lobes by some means.

Our results are clearly different from those of Kaiser et al. (2000), who used a non-relativistic ram-pressure balance equation. Since the inner double expansion speed cannot be more than c, Kaiser at al. (2000) had to restrict their ambient medium density for the inner double. They cut off the curves (in their Fig. 1), representing the variation of ambient medium density vs. jet power below a certain density of the ambient medium. In their Fig. 1, the continuous curves describing the amount of cocoon matter density that is available from the $e^- e^+$ jet supply does not intersect with the dashed curves describing the ambient medium density that can reproduce the observed properties of the inner doubles for many DDRGs, which has the effect that the jet is completely ballistic, if there is only jet supplied matter in the cocoon. As a consequence, there is no hotspot formation (and perhaps no confinement of the inner lobes as well). However, this is an artefact of the application of the nonrelativistic equation [see equation (11) of Kaiser & Alexander (1997)] for the momentum balance at the jet head. Whatever may be the ambient medium density, the jet head can propagate at most at the speed of the jet bulk motion as the ambient medium density tends to zero. So ideally, in a correct model, the jet head speed, $\beta_{\rm h}$ should gradually approach $\beta_{\rm j}$ in the limit that $\rho_{\rm a} \to 0$. This is definitely not the case in the model of Kaiser et al. (2000). Because of their nonrelativistic approach, the Kaiser et al. model artificially needs more cocoon density to explain the observed hotspot formation and lobe confinement of the inner double. In our model of momentum balance, it is quite clear from equation (8) that when $\rho_{\rm a} \to 0$, $\eta \to 0$; therefore, $\beta_{\rm h} \to \beta_{\rm j}$, hence our model has the correct behaviour in the limit. Our fully relativistic equation (8) for momentum balance, for $\beta_{\rm h} \to 0$ limit for denser $w_{\rm a}$, reduces to the widely used ram pressure balance equation, $v_{\rm h} = \sqrt{\frac{Q_{\rm j}}{cA_{\rm h}\rho^0}}$.

We emphasise again that we do not rule out the possiblity of a small amount of thermal matter entrainment/ingestion into the cocoons of radio galaxies; low-frequency polarization observations are required to search for it and the results can then be compared to those of models such as those we present here.

4.5.5 The hotspot motion of inner doubles is relativistic

It is evident from the bottom panel of Fig. 2 that many of the DDRGs we have studied for our injection index related physics have outer jet powers greater than 10^{44} erg s^{-1}. As we will argue in Section 5 the similarity of the injection indices (top panel of Fig. 2) in the outer and inner doubles suggests that the inner and outer jets have similar power, so that it is reasonable to assume that our DDRGs have *current* jet powers of order 10^{44} erg s^{-1} or higher. In this section we focus on DDRG with these jet powers, since we have observational data to constrain our theoretical models. For the small sample of DDRGs that we have studied in our previous two papers (Konar et al. 2012, 2013) the typical magnetic field is $\gtrsim 5$ μG (except J0116-4722 which has ~ 0.27 μG). This justifies the assumption in Section 4.5.4 of a jet power of 10^{44} erg s^{-1} and a magnetic field of 5 μG in the ambient medium.

Our work in Section 4.5.4 shows that the hotspots of the inner jets have to travel at a the relativistic speed (see Fig. (4) and (5)), provided there is no significant entrainment/ingestion of thermal matter into the outer cocoon. We therefore predict that a relativistic beaming (or de-beaming) effect should be visible in the approaching (receding) hotspots of inner doubles. The JTS in our radio images, with a resolution of a few arcsec ($\sim$ 10 kpc) will be seen as a point source. It follows that any jet head emission can be thought of as two components: one is a point source component (the JTS), the other is the diffuse component which is the injected downstream plasma backflowing into the inner lobes. The beaming (or de-beaming) effect should be prominently visible in the point source component. As a result the inner jet-head which is approaching us should look like a round standard hotspot and the inner jet-head which is receding from us will have a shape more like the bow shock. Of course, to test this prediction we need observations with an angular resolution which is enough to resolve our predicted structure, and yet does not resolve out the diffuse component with the given sensitivity of the telescope. We show high-resolution images of the inner doubles of a few DDRGs in Fig. 6, which, while obviously not constituting a rigorous test of the model, show qualitative agreement with our predictions, in the sense that one side of each source has a more convincing compact hotspot than the other (coincidentally, the S side in each of the three images shown here has the more compact hotspot). We note that a pure relativistic model would also predict that the approaching lobe

would also be longer, due to light-travel-time effects, which we do not observe here. In the framework of the model, this would have to be explained in terms of inhomogeneities in the outer cocoon material.

To investigate the Mach number in the inner doubles further, we have made a high resolution image of the inner double of J1453+3308 from the VLA archival data taken at C-band and with the A-array. As shown in Fig. 7, the inner northern lobe shows a clear conical structure. We estimate that the half angle of the cone is 15.86°, which means that the relativistic Mach number would be $M_{\rm rel} = 1/\sin(15.86) = 3.65$. This is consistent with the idea that the northern lobe is a relativistic shock. Sophisticated modelling, beyond the scope of the present paper, would be required to find the possible thermal matter content within the outer lobes from this estimate of $M_{\rm rel}$.

5 DISCUSSION

In the preceding section, we have addressed the theoretical aspects of the inner jet dynamics of DDRGs. Keeping in mind the inner jet dynamics and the theory of particle acceleration at the relativistic MHD shock, we discuss the interpretation of our observational results in this section.

5.1 Injection index and DDRGs

It is *a priori* quite surprising that the injection index is so similar between the two episodes of DDRG activity. Analytical modelling of particle acceleration at strong shocks suggests that the principal factor determining the injection index should be the strength of the JTS and the JTS strength depends on the proper speed of the upstream fluid ($\Gamma_{\rm j,hs}\beta_{\rm j,hs}$) as measured in the shock frame, i.e., hotspot frame (see Kirk et al. 2000). The relativistic velocity addition law yields

$$u_{\rm j,hs} = \Gamma_{\rm j,hs}\beta_{\rm j,hs} = \Gamma_{\rm j}\Gamma_{\rm hs}(\beta_{\rm j} - \beta_{\rm hs}), \qquad (23)$$

where $u_{\rm j,hs}$ is the proper velocity or the spatial components of the four velocity of the jet fluid as measured from the hotspot frame, $\Gamma_{\rm j,hs}$ is the Lorentz factor corresponding to the bulk speed, $\beta_{\rm j,hs}$ (in units of c) of the jet fluid as measured from the hotspot frame. From this equation, it is clear that the shock strength depends on $\beta_{\rm hs}$, the hotspot advance speed. Therefore, the JTS strength should depend on the ambient medium density ($\rho_{\rm a}$), as $\beta_{\rm hs}$ depends on $\rho_{\rm a}$ through ram pressure balance at the contact discontinuity at the head of the lobe. However, if the ambient medium consists of relativistic particles, as it does for the inner jets of the DDRGs, where the ambient medium is the cocoon material of the outer doubles, then $\rho_{\rm a} = \frac{\varepsilon}{c^2}$, where ε is the relativistic internal energy density which contains the rest mass energy also, and c is the speed of light. This should be at least two orders of magnitude less (Brocksopp et al. 2007, 2011; Safouris et al., 2008; Clarke & Burns, 1991) than that of the thermal ambient medium through which the outer jets had propagated. $\beta_{\rm hs}$ should accordingly be faster in the inner hotspots, and the JTS is expected to be weaker than that in the previous episode, assuming constant $\beta_{\rm j}$ and $Q_{\rm j}$, an assumption that we revisit below. We might therefore naively expect to see systematic differences between the injection indices in the two lobes in DDRG, in the sense that $\alpha_{\rm inj}$ in the inner doubles compared to the outer doubles, which is not what we observe (except possibly in the case of 3C293: see Fig. 2)

What can account for this discrepancy between observation and expectation? Since the strength of the JTS depends on the proper speed (or the spatial components of the four-speed, $u_{\rm j,hs} = \Gamma_{\rm j,hs}\beta_{\rm j,hs}$) of the upstream jet flow as measured in the hotspot frame, it is worth estimating the proper velocities, $u_{\rm j,hs}$, of the upstream jet flow for a fixed $\Gamma_{\rm j} \sim 2$ (see Mullin & Hardcastle 2009) and a range of hotspot velocities, $\beta_{\rm hs}$. For the classical double radio galaxies (which are equivalent for the outer double of DDRGs) the hotspot velocities range from $0.05-0.1c$ (Konar et al. 2009; Jamrozy et al. 2008; Scheuer 1995) and for the inner doubles the hotspot velocities range from $0.05-0.5c$. The lower limit is not a very stringent limit which is suggested by our data, published by Konar et al. (2012; 2013), on the lower limits on the break frequency in the synchrotron spectra of inner doubles. Since most of the sources do not have deep images at frequencies greater than 8.4 GHz, we cannot directly measure the break frequencies or even place a very stringent limits in break frequency. The upper limit on the inner hotspot speed is from Safouris et al., (2008). Assuming $\Gamma_{\rm j} \sim 2$, which corresponds to $\beta_{\rm j} \sim 0.866$, the application of equation (23) yields values of $u_{\rm j,hs}$ of 1.634, 1.539 and 0.665 for $\beta_{\rm hs}$ values of 0.05, 0.1 and 0.5 respectively. For the outer doubles, with their low hotspot advance speeds, we find $1.539 \gtrsim u_{\rm j,hs} \gtrsim 1.634$, i.e. a very similar proper velocity; for speeds as high as the upper limit on $\beta_{\rm hs}$ for the inner doubles, the proper velocity is much lower and so the JTS would be expected to be weaker. We conclude that if the injection index−jet power correlation observed in classical FR IIs were purely due to JTS strength, then the injection indices of the inner doubles should have been steeper in all DDRGs, as inner hotspots are very likely to move faster than their outer counterparts. However, this is not what we observe.

There are two possibilities to explain these observations: either (i) the jet bulk Lorentz factor has such a high value that the difference between inner and outer double in $\beta_{\rm hs}$ does not cause significant difference in shock strength and injection index, or (ii) standard DSA models in the relativistic regime do not actually describe the hotspots. We prefer the former possibility. Our study of momentum balance at the jet head in Section 4.5.4 shows that the formation of JTSs and bow shocks in inner jets is quite plausible even if the ambient medium is a tenuous nonthermal medium with no external thermal matter ingested into it. Of course, $u_{\rm j,hs}$ will be different for inner and outer jets during their active phase; however, if the jet Lorentz factor is high enough then the JTSs in both outer and inner jets will produce the universal (true) injection index of 0.62 (Kirk et al. 2000), which will then be steepened (by synchrotron losses) by the same amount when the plasma comes out of the hotspots (to produce the same observed injection index) provided the jet powers are the same in both episodes. The higher the jet Lorentz factor, easier will be to explain the $\alpha_{\rm inj}^{\rm inn} - \alpha_{\rm inj}^{\rm out}$ correlation. We explore this type of model in the following subsections.

5.2 Jet power and injection index

Fig. 2 shows that there is a strong correlation between jet power and injection index in radio galaxies in general, including some of the outer lobes of our DDRG sample. This observation prompts two questions: (i) can this correlation account for the correlation between the injection indices in the inner and outer doubles in the DDRG sample, and (ii) how do these correlations arise?

First of all, it is worth considering what determines the jet power of a radio galaxy and whether any of the parameters in question are expected to change between different episodes of activity. In general, we expect the jet power to depend on properties of

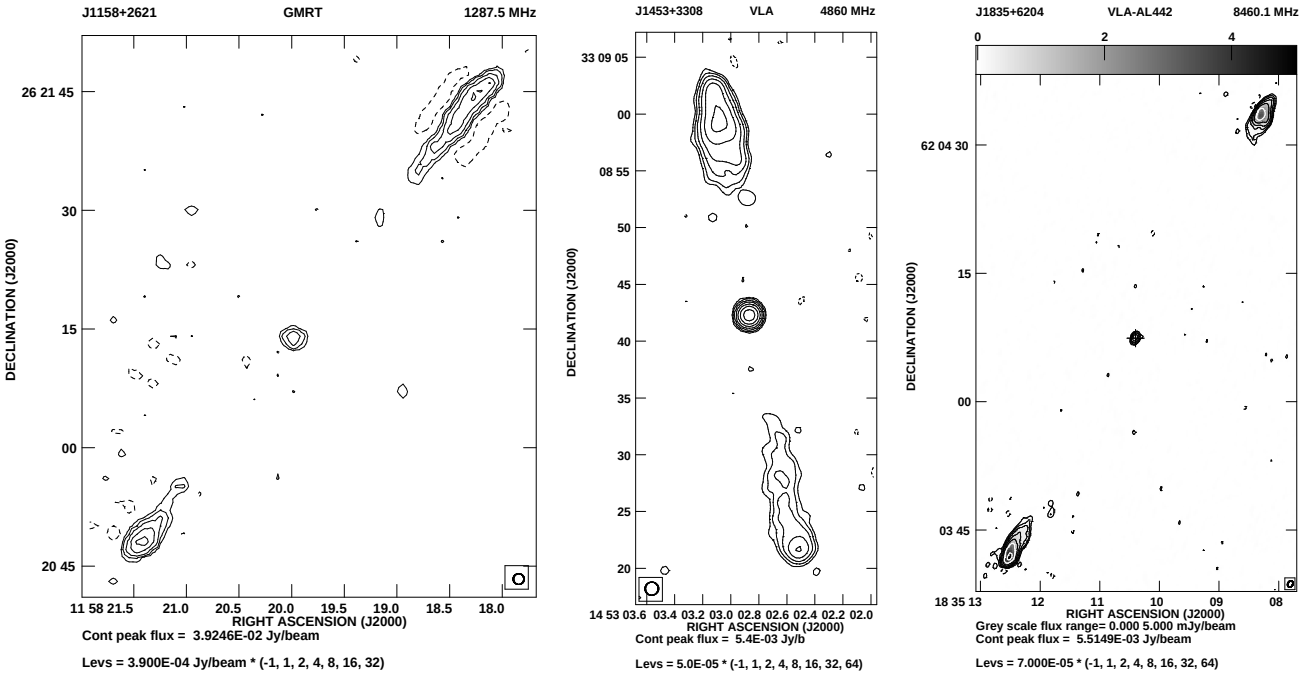

Figure 6. The inner doubles of a few DDRGs. The source name, telescope name and observed frequency are given at the top of each image. The peak flux density, the countour level are given at the bottom of each image. An ellipse within a square box at the bottom left or right corner is the resolution of the radio image. Left panel: This has been made with the GMRT data (project code: 10CKa01) with 20 kλ lower cutoff. This image has a resolution of 1.36×1.36 arcsec^2. Middle panel: This image is reproduced from Konar et al. (2006). Right panel: This image has been made with the VLA archival data (project code: AL442) and has a resolution of 0.79×0.57 arcsec^2 at a position angle of $\sim 336°$.

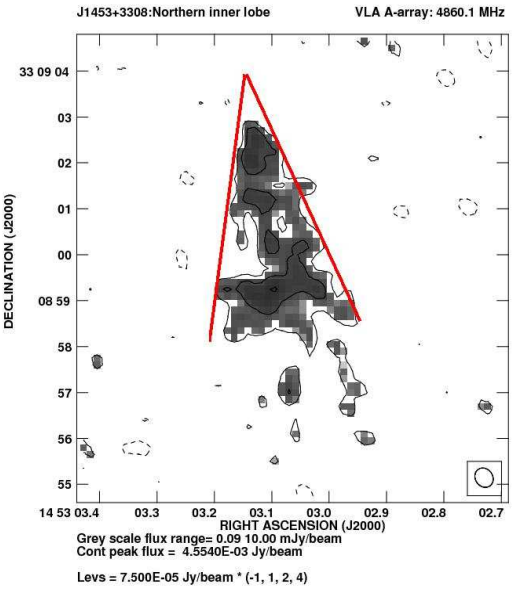

Figure 7. The inner northern lobe of J1453+3308. This is a C-band, A-array image with resolution 0.44×0.38 arcsec^2 at Position angle of 36.03°. The proposal code of the data is AS697.

the accretion system such as the black hole mass $M_\bullet$, the accretion rate $\dot{M}$ and perhaps the black hole spin $S_\bullet$ (e.g. Blandford & Znajek 1977; Bhattacharya, Ghosh & Mukhopadhyay 2010). Other parameters set by the jet generation mechanism, such as the ratio (σ_j) of magnetic enthalpy density ($w_B = \frac{B^2}{4\pi}$) to particle enthalpy density (Kirk et al. 2000) may also play a role.

Can the black hole of a DDRG increase significantly during the quiescent phase of jet forming activity? If we assume that during the quiescent phase of jet forming activity, the AGN accretes and radiates efficiently, then we can assume the canonical values of $\lambda = 0.1$ and $\xi = 0.1$. Radio galaxies are supposed to be produced by black holes of mass $\gtrsim 10^8 M_\odot$ (Chiaberge & Marconi 2011). For a SMBH of $M_\bullet = 10^8 M_\odot$ and the time scale of quiescent phase of jet forming activity of 10^7 yr (or less for our sample of sources), the SMBH will increase its mass by $\Delta M = 2.27 \times 10^6 M_\odot$ (using equation C4 in Appendix C). This is much smaller than the initial black hole mass which is $10^8 M_\odot$. This calculation is done for the higher end of the range of the quiescent phase and with the assumption that the AGN accretes efficiently via thin-disk accretion mode during this phase, and so is likely to be an overestimate for a typical DDRG. Therefore, it is clear that mass accretion cannot significantly change $M_\bullet$ of the central SMBH during the time scale of the quiescent phase which ranges from $\sim 10^5$ yr to a several tens of Myr (Konar et al. 2013; 2012; 2006; Saikia et al., 2006).

Since the DDRGs we are concerned are all powerful FR II sources and are high excitation radio galaxies, they are thought to be accreting via a standard accretion disk (e.g. Hardcastle, Evans & Croston 2006). Matter constantly loses angular momentum via the disk to fall into the black hole. However, inside the Innermost Stable Circular Orbit (ISCO), there is no stable orbit. The matter should thus fall from the ISCO to the SMBH with the angular momentum corresponding to the Keplerian motion at the ISCO. This assumption should give us an upper limit on the angular momentum deposited into the SMBH during the quiescent phase. We estimate the maximum angular momentum deposited in the following way. We assume that the ISCO is at $3R_s$, where $R_s = \frac{2GM_\bullet}{c^2}$ is

the Schwarzschild radius. If the black hole spins, the ISCO is supposed to be smaller, however our estimation of angular momentum with $3R_s$ will give an upper limit, which we are interested in. As long as the quiescent phase of jet forming activity is $\lesssim 10^7$ yr, we do not expect that the SMBH at the central engine will accumulate any substantial amount of amgular momentum which will change the jet power significantly (see Appendix C). This result will hold for any SMBH with any mass higher than $10^8 M_\odot$ for the same values of the other parameters. Therefore, it is likely that $M_\bullet$ and $S_\bullet$ do not change dramatically in two episodes of jet forming activity, unless there is a merger with another galaxy (Schoenmakers et al. 2000a), or SMBHs in a comparable-mass binary coalesce between two episodes (Liu et al. 2003). However, the stability of the jet axis (Konar et al. 2006; Saikia et al. 2006) between the two episodes and the duration of the quiescent phase of the DDRGs (Konar et al. 2012, 2013) are not at all favourable for a merger with another galaxy (merger time scale $\sim 10^9$ yr). SMBH coalescence in unequal mass binary is quite plausible between the two episodes, provided that the merging black hole is small enough to maintain the stability of the jet axis between the two episodes, but, as a consequence of that restriction, this also does not affect $M_\bullet$ and $S_\bullet$. Finally, we note that if the quiescent phase is due to lack of fuel (i.e. a large drop in $\dot{M}$), it is clear that $M_\bullet$ and $S_\bullet$ must remain unchanged in the two episodes of jet forming activity.

We have little direct information on σ_j, but for the kpc/Mpc-scale sources the lobes and hotspots are close to equipartition (Croston et al. 2005; Hardcastle et al. 2004), i.e. $\sigma \sim 1$. It is plausible that the jet fluid is also in equipartition. This means $\sigma_{\rm j}$ should be ~ 1 in both the episodes.

The factor that can most easily change between the two episodes is the fuel supply, $\dot{M}$. If the black hole is accreting from the hot-gas environment, the accretion rate is expected to be determined by the central cooling time, which is $\sim 10^8$ yr, so that the density of hot gas is unlikely to change during the quiescent phase that we have determined for these FR II DDRGs (though we note that Jetha et al. (2009) report on a low-power system thought to be powered by hot-gas accretion where the quiescence timescale is indeed $\sim 10^8$ yr). But in a scenario where the fuel supply comes from cold gas, the timescale for significant variations can be comparable to the Keplerian timescale for the torus, which could be $< 10^6$ yr. There thus seems to be no physical reason why $Q_{\rm j}$ should be correlated between different epochs of jet forming activity. However, in fact, there is a very strong selection effect requiring the two values of $Q_{\rm j}$ to be at least comparable in the objects we study: if they are very different, we will not observe a classical DDRG in which the inner and outer doubles are of comparable luminosity. Thus, if we can explain why $Q_{\rm j}$ controls the injection index, we can explain the observed correlation between the injection indices of the two epochs in terms of a correlation between their values of $Q_{\rm j}$.

We discuss in this section the mechanism by which jet power can affect the injection index. First of all, as noted above, DSA models predict that the original power law index will depend on the shock strength. A higher jet power implies a higher jet momentum flux, which will drive a faster expansion of the lobe (higher $\beta_{\rm hs}$) for a given external density, and so would actually weaken the jet termination shock, giving injection index. This weakening of JTS by higher $Q_{\rm j}$ will work while $\Gamma_{\rm j}$ is not very high, because for very high $\Gamma_{\rm j}$ the $\beta_{\rm j,hs}$ will always be very close to 1, no matter what the value of $\beta_{\rm hs}$ is. So, in the high-$\Gamma_{\rm j}$ regime, if a higher jet power implies a higher jet bulk *speed* ($\beta_{\rm j}$) then the JTS will be stronger and higher jet power will imply flatter injection index. There are some observational constraints on this possibility: Mullin & Hardcastle (2009) recently found no statistical correlation between radio power and $\Gamma_{\rm j}$ for a complete sample of 98 FR II sources with $z < 1$ spread over a monochromatic luminosity range of ~ 3 orders of magnitude at 178 MHz. Taken at face value, these results imply that the jet bulk speed for large source sizes (as studied by Mullin & Hardcastle) is independent of the jet power, and the $\Gamma_{\rm j}$ (~ 2) is not very high. This in turn implies, by the argument of Section 5.1, that the shock strength might *decrease* for higher jet power, which is in the sense required by the observations. This can explain, at least qualitatively, the jet power$-$injection index correlation, relying on the assumptions that (i) the jet speed across the cross section is the same and close to the directly estimated value of $\Gamma_{\rm j}$ (e.g., ~ 2) and (ii) the external density is the same for all sources (though this is probably not the case). However, it certainly fails to explain the similar injection index in two episodes for the following reasons. The dynamical modelling of Inner doubles of J1548-3216 by Safouris et al. (2008) and the conical shape (which is reminiscent of a bow-shock) of the inner northern lobe head of J1453+3308 (see Fig. 6) as shown by Konar et al (2006) suggest much faster hotspot velocity and tenuous ambient medium density compared to the outer doubles (yet the injection index of the inner doubles are similar to that of the outer doubles). This can only be possible if the principal parameters that injection index depend on, e.g., $Q_{\rm j}$, $\sigma_{\rm j}$ and $\rho_{\rm a}$, have adjusted values so as to cause no change in injection index in the two episodes. Clearly, this is highly unlikely. Therefore, lower value of $\Gamma_{\rm j}$ cannot explain the observations at all.

If the model described by Kirk et al. (2000) describes the particle acceleration phenomena at the hotspots, then a possible curve of the kind shown in Fig. 4 of their paper (the top panel of Fig. 8 of this paper), but with an appropriate value of $\sigma_{\rm j}$ (i.e., $\sigma_{\rm j}$ at equipartition) with a very high Lorentz factor flow of jet fluid, combined with higher synchrotron losses due to higher magnetic field at the hotspots of high power sources, can explain the injection index$-$jet power correlation as well as the the similarity of injection index in two different episodes. However, keeping in mind the low Lorentz factor jets suggested by Mullin & Hardcastle (2009), we hypothesize a structured jet with a fast moving spine inside the jets, the bulk of the jet kinetic power is concentrated in the spine and thus it dominates the dynamics and the particle acceleration[4]. To be consistent with Fig. 4 of Kirk et al. (2000), the spine can be moving with very high Lorentz factor ($\gtrsim 10$) and outer layers denser than the spine of the jets move slower so as to produce a lower Lorentz factor (e.g. ~ 2) as estimated by Mullin & Hardcastle (2009). Since the particles from the high Lorentz factor spine are accelerated at the JTS, the ambient medium density does not affect the value of injection index provided that the jet power (with jet fluid being in equipartition) remains same in both episodes. We have plotted the curves showing the variation of $u_{\rm j,hs}$ (and $u_{\rm h}$) vs. $n_{\rm a}$, i.e., the number density of particles in the ambient medium for two different values of the Lorentz factor (5 and 50) keeping the same jet head radius of 0.5 kpc and the values of the other parameters. Since from Kirk et al. (2000) (see top panel of Fig. 8), it is clear that for any value of magnetic field strength in the relativistic plasma, the upstream proper speed of the plasma in the shock frame has to be at least greater than 10 to attain the universal injection index. We require

[4] In a completely independent argument, Hardcastle (2006) argues that to model the jet related X-ray emission of core-dominated radio loud quasars as inverse-Compton scattering of Cosmic Microwave Background (CMB) photons, the jet has to have velocity structure and the spine of the jet should have $\Gamma_{\rm j} \gtrsim 15$. This is fully consistent with our results.

Table 2. Source parameters that are employed in plotting $\alpha_{\rm inj} - Q_{\rm j}$ (in Fig. 2) and $\alpha_{\rm inj} - z$ correlations respectively. The component designations are N-lobe (S-lobe) is the northern (southern) lobe, NW-lobe (SE-lobe) is the North-western (south-eastern) lobe, Int-core is the core subtracted integrated source. The description of the columns is as follows. Column 1: source name, Column 2: Alternative name, Column 3: redshift of the host galaxy, Column 4: injection spectral index of the radio galaxies, Column 5: jet power and Column 6: reference and comment.

Source	Alt. name	z	$\alpha_{\rm inj}$	$Q_{\rm j}$ (10^{45} erg s^{-1})	Ref. and comment
(1)	(2)	(3)	(4)	(5)	(6)
DDRGs††			$\alpha_{\rm inj}^{out}$	Q_j^{out}	
J0041+3224	B2 0039+32	0.45†	0.756	0.9315	1
J0116-4722	PKS 0114-47	0.14610	0.618	$*$	2
J0840+2949	4C 29.30	0.064715	0.810	$*$	3
J1158+2621	4C +26.35	0.112075	0.788	0.1656	2
J1352+3126	3C293	0.045034	0.855	$*$	4
J1453+3308	4C 33.33	0.248174	0.568	0.3156	5
J1548-3216	PKS 1545-321	0.1082	0.567	0.1934	6
J1835+6204	B1834+620	0.5194	0.818	2.8520	1
Large radio galaxies			$\alpha_{\rm inj}$	Q_j	
J0135+3754 Int-core	3C46	0.4373	0.982	13.71	7
J0912+3510 N-lobe		0.2489	0.560	0.12	8
J0912+3510 S-lobe		0.2489	0.628	0.33	8
J0927+3510 NW-lobe		0.55†	0.750	2.00	8
J0927+3510 SE-lobe		0.55†	0.700	2.36	8
J1155+4029 NE-lobe		0.53†	0.876	5.94	8
J1155+4029 SW-lobe		0.53†	0.838	1.42	8
J1313+6937 NW-lobe		0.106	0.610	0.16	8
J1313+6937 SE-lobe		0.106	0.610	0.15	8
J1343+3758 NE-lobe		0.2267	0.570	0.25	8
J1343+3758 SW-lobe		0.2267	0.570	0.41	8
J1604+3438 W-lobe		0.2817	0.554	0.13	8
J1604+3438 E-lobe		0.2817	0.554	0.13	8
J1604+3731 NW-lobe		0.814	0.765	2.71	8
J1604+3731 SE-lobe		0.814	0.775	3.39	8
J1702+4217 NE-lobe		0.476	0.588	0.64	8
J1702+4217 SW-lobe		0.476	0.588	0.59	8
J2245+3941 Int-core	3C452	0.0811	0.782	1.03	7
J2312+1845 NE-lobe	3C457	0.427	0.820	5.59	8
J2312+1845 SW-lobe		0.427	0.820	2.37	8

$*$: No definite age estimate exists, only a limit, so the source is not plotted.
†: Estimated redshift.
††: For DDRGs, we have considered the outer double for the $\alpha_{\rm inj} - Q_{\rm j}$ and $\alpha_{\rm inj} - z$ correlation.
1: Konar et al. (2012), 2: Konar et al. (2013), 3: Jamrozy et al. (2007), 4: Joshi et al. (2011), 5: Konar et al. (2006), 6: Machalksi et al. (2010), 7: Nandi et al. (2010), 8: Jamrozy et al. (2008).

the universal injection index to be obtained by all sources in order to explain the observed similar injection index in two episodes of DDRGs; otherwise, there has to be an adjustment of the parameter values to produce similar observed injection indices in the two episodes for our sample of DDRGs. For a jet head radius of 0.5 kpc, the spine of the jet has to have $\Gamma_{\rm j} > 50$ to produce the upstream jet speed of $\Gamma_{\rm j,hs} > 10$ for our study of the realistic case of a hypothetical DDRG (see Fig. 8).

The jet power of FR II sources spans 3 to 4 orders of magnitude ($\sim 10^{43} - 10^{47}$ erg s^{-1}), while it appears that $\Gamma_{\rm j}$ may vary only within a small range, as Mullin & Hardcastle (2009) find no evidence for a correlation between bulk Lorentz factor and jet power. This means that higher jet power in stronger sources cannot be produced solely by an increase in the jet Lorentz factor. Instead, higher powers must be a result of higher energy density in the jets, which implies higher energy densities in the post-JTS jet matter. Since observations imply that hotspots are close to equipartition (e.g. Hardcastle et al. 2004) this also implies higher magnetic field strengths in the hotspots, with consequently stronger synchrotron losses in the regions of particle acceleration. This gives a way in which the jet power may affect the injection index. Hardcastle et al. (2004) and Brunetti et al. (2003) argue, based on X-ray and optical observations, that both the high-energy cutoff and the break energy of the electron energy spectrum in the hotspots are affected by the hotspot magnetic field strength. If the hotspot break frequency is low enough that adiabatic expansion can shift it down below the lowest frequency we observe (usually ~ 20 MHz), then we expect to see an increased injection index, though we would predict a spectral flattening at still lower frequencies. For a break frequency around the optical/IR, we require one-dimensional adiabatic expansion factors $\gtrsim 30$ to bring the hotspot break frequency down to hundreds of MHz, which is by no means implausible.

The existence of correlations between the monochromatic radio luminosity L_ν, the source redshift z, and the low-frequency spectral index α for radio galaxies have been known for some time (Laing & Peacock 1980). Since a higher $Q_{\rm j}$ produces higher radio power in a source, our discussion above suggests that the $\alpha - L_\nu$ correlation is the primary one, and is driven by our pro-

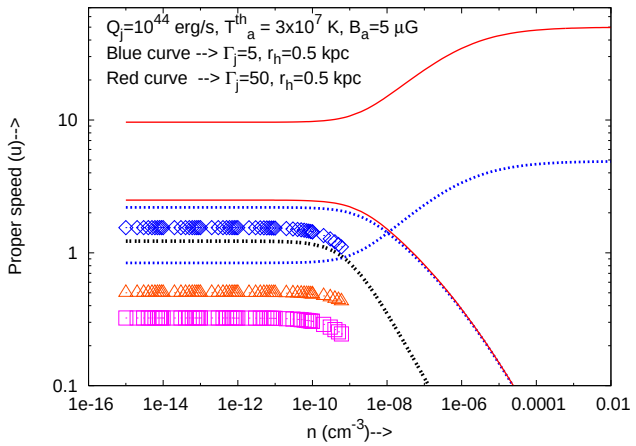

Figure 8. Plots as in Fig. 5 for high bulk Lorentz factor jets. The red curves are for $\Gamma_{\rm j} = 50$. See the caption of Fig. 5 for the colours, symbols and descriptions. The parameter values are annotated in the plot.

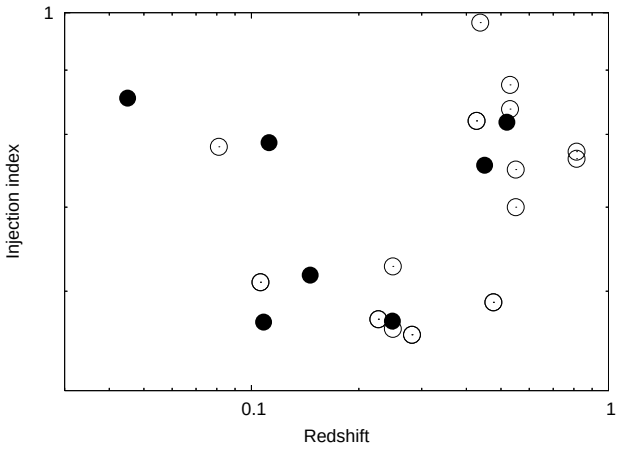

Figure 9. $\alpha_{\rm inj}$ vs. z plot for the same sample of sources as in Fig. 2. Symbols have the same meaning as in Fig. 2. No correlation is evident.

posed $\alpha_{\rm inj} - Q_{\rm j}$ correlation. In a flux-limited sample L_ν and z are correlated, so the $\alpha - z$ correlation automatically arises. The fact that $\alpha - L_\nu$, or in a new guise $\alpha_{\rm inj} - Q_{\rm j}$ is the primary correlation is further supported by the absence of any correlation between $\alpha_{\rm inj}$ and z for the sample that we use in this paper (see Fig. 9).

We emphasise that the preceding discussion is based on the assumption that particle acceleration takes place predominantly at the JTS. As noted in Section 1, some particle acceleration certainly does occur in the pc- and kpc-scale jets, and while similar arguments to those given above may apply to the acceleration regions in the jets, we do not know enough about the acceleration mechanism for a detailed analysis. If the jets' initially ultrarelativistic speeds persist to large distances, as we suggest above, then it is hard to see how particle acceleration in the jet can have a significant effect on the post-JTS spectrum; moreover, for an ultrarelativistic shock, the state of the downstream plasma is essentially independent of that of the upstream plasma so long as the latter does not have a very high internal energy density[5] (Kirk et al. 2000). While we cannot rule out an effect of jet-related particle acceleration, we can construct a self-consistent model in which it is unimportant.

5.3 Testable predictions

From our estimation, from equation (C4) and (C13), of total mass accumulation and change in spin parameter a, for a central SMBH of with initial mass $\gtrsim 10^8 M_\odot$, due to accretion can be significant if the SMBH accretes efficiently over a time scales of a few 10^8 yr or more. Though the exact dependence is not known, the jet power is thought to depend on $M_\bullet$ and a. Therefore, if the initial mass of a SMBH in any radio galaxy is $\gtrsim 10^8 M_\odot$ (all radio galaxies are supposed to have $M_\bullet \gtrsim 10^8 M_\odot$: Chiaberge & Marconi 2011) and the duration of quiescent phase of jet activity is a few times 10^8 yr or more, we might be able to find significantly different values of injection spectral index in the two episodes. Since the fundamental parameters that the jet power, $Q_{\rm j}$ is expected to depend on are $M_\bullet$ and a, any change in these parameters by any means should be in principle reflected in different values of the injection index in two different episodes of a radio galaxy. In misaligned DDRGs, the jet axes are changed significantly. Therefore, it is quite natural to think that some large scale perturbation has affected the central SMBH. Hence we are likely to see significantly different values of injection index in two different episodes. As per our expectation, we do see a significant difference in the values of the injection index in two consecutive episodes of the misaligned DDRG, 3C293. The error bars are smaller than the deviation from the equality line. While this needs to be verified with a larger sample, this is certainly consistent with our prediction. The error bars of J0116-4722 (an aligned DDRG) are consistent with the injection indices being similar in the two episodes.

From our detailed theoretical and observational studies we conjecture that the DDRGs with $\Gamma_{\rm j} \lesssim 10$ (if they exist) are likely to have dissimilar injection index in two episodes, even though $\Gamma_{\rm j}$ and $Q_{\rm j}$ are same in both episodes. The reason is that $\Gamma_{\rm j,hs}$, and hence the Mach number of the JTS, will be different in the two episodes, which leads to different injection indices. Though Mullin & Hardcastle (2009) suggest similar $\Gamma_{\rm j}$ for all FR II sources, they cannot completely rule out different $\Gamma_{\rm j}$ for different sources. They look at the slowest outer layer components of jet which may show up with the same/similar speed even in the presence of variation in the Lorentz factors of jet spines, hence a range of $\Gamma_{\rm j}$ values for the spines of the jets might not be detected in their study. There could be very low-power FR II sources which have low Lorentz factor (< 10) spine of their jets. If they are episodic then we predict that they should show dissimilar injection indices in the two episodes.

Finally, there is no real reason why DDRG with very different jet powers in the two episodes (due to a significant change in $\dot{M}$) should not exist in our model; they are just observationally difficult to detect since the inner and outer lobes would be expected to have very different luminosities/surface brightnesses. Sensitive low-frequency surveys with the GMRT and LOFAR might detect such objects in the future and our prediction is that large differences in the jet power in the two episodes will give rise to large differences in the measured injection indices.

[5] For the fast moving spine of the jet with moderate bulk Lorentz factor of 4, we have shown in Appendix D that the internal energy density is negligible compared to the bulk kinetic energy density of the spine of the jet

6 SUMMARY AND CONCLUSIONS

We have discovered a new property of episodic (double-double) FRII RGs, which allows us to draw many other inferences which may be summarized as follows.

(i) We have discovered that the values of injection index (the low-frequency power-law index of synchrotron emission) are similar in the two different episodes for most of the DDRGs in our sample.

(ii) This observational result means that the injection index doesn't appear to bear any relation to the medium into which the lobe is expanding. However, our sample (and previous work) show that it is strongly dependent on the jet power.

(iii) Point (ii) implies that the injection index over the entire duration of the active phase of a radio galaxy should be the same or similar provided the jet power remains constant, even though the lobes are interacting with an ambient medium of strongly varying density.

(iv) We have provided explicit, consistent relativistic formulae for the momentum balance at the jet head (equation 8) and thus for the dynamics of the radio lobes in both episodes of the DDRG activity. We argue that observations favour e^-e^+ plasma rather than e^-p^+ plasma.

(v) We argue that the jet power in the two episodes of a DDRG needs to be the same, or at least similar, with the same or similar Lorentz factor and internal energy, in order to produce a similar injection index in both episodes without fine-tuning of other parameters governing the jet properties. An observational selection effect helps to enforce this condition in existing samples of DDRG.

(vi) Our models imply that the $\alpha - L_\nu$ correlation of a flux limited sample of RGs is the primary one, and not the $\alpha - z$ correlation, and require that higher-power RGs do not have $\Gamma_{\rm j}$ but rather higher jet-frame energy density, consistent with observation. There may be a simple scaling relationship between the energy density in the jet and the accretion rate $\dot{M}$ for a radio-loud source..

(vii) We predict/conjecture that DDRGs with long quiescent phase, misaligned doubles, low jet Lorentz factors (< 10) or significant changes in jet power between the two episodes are more likely to have dissimilar injection indices in two episodes of jet forming activity. These predictions can be tested observationally.

ACKNOWLEDGMENTS

This research has made use of the NASA/IPAC extragalactic database, which is operated by the Jet Propulsion Laboratory, Caltech, under contract with the National Aeronautics and Space Administration. We thank the GNU/Linux group for their contribution. CK acknowledges Ronald Taam for discussion on various theoretical issues. CK also thanks the School of Physics, Astronomy and Mathematics at the University of Hertfordshire, where a part of this research was done, for their hospitality. CK acknowledges the grant (No. NSC99-2112-M-001-012-MY3) from the National Science Council, Taiwan.

REFERENCES

Anile A.M., 1989, Relativistic Fluids, and Magneto-Fluids (Cambridge Univ. Press)
Balmaverde B, Baldi R.D., Capetti A., 2008, A&A, 486, 119
Bell A.R., 1978a, MNRAS, 182, 147
Bell A.R., 1978b, MNRAS, 182, 443
Bhattacharya D., Ghosh S., Mukhopadhyay B., 2010, ApJ, 713, 105
Bicknell G.V., 1994, ApJ, 422, 542
Bicknell G.V., 1995, ApJS, 101, 29
Blandford R.D., Znajek R., 1977, MNRAS, 179, 433
Brunetti G., Mack K.-H., Prieto M.A., Varano S., 2003, MNRAS, 345, L40
Capetti A., Zamfir S., Rossi P., Bodo G., Zanni C., Massaglia S., 2002, A&A, 394, 39
Chiaberge M., Marconi A., 2011, MNRAS, 416, 917
Chou M., Hau L.-N., 2004, ApJ, 611, 1200
Clarke D.A., Burns J.O., 1991, ApJ, 369, 308
Croston J.H., Birkinshaw M., Hardcastle M.J., Worrall D.M., 2004, MNRAS, 353, 879
Croston J.H., Hardcastle M.J., Harris D.E., Belsole E., Birkinshaw M., Worrall D.M., 2005, ApJ, 626, 733
Croston J.C., Hardcastle M.J., Birkinshaw M., Worrall D.M., Laing R.A., 2008, MNRAS, 386, 1709
Dunn R.J.H., Fabian A.C., Celotti A., 2006, MNRAS, 372, 1741
Dennett-Thorpe J., Scheuer P.A.G., Laing R.A., Bridle A.H., Pooley G.G., Reich W., 2002, MNRAS, 330, 609
Fanaroff B.L., Riley J.M., 1974, MNRAS, 167, 31
Floyd D.J.E., Perlman E., Leahy J.P., Beswick R.J., Jackson N.J., Sparks W.B., Axon D.J., O'Dea C.P., 2006, ApJ, 639, 23
Gedalin M., 1993, Phys. Rev. E., 47, 4354
Gopal-Krishna and Wiita P.J, 1990, A&A, 236, 305
Hardcastle M.J., 2006, MNRAS, 366, 1465
Hardcastle M.J., Croston J.H., Kraft R.P., 2007, ApJ, 669, 893
Hardcastle M.J., Evans D.A., Croston J.H., 2006, MNRAS, 370, 1893
Hardcastle M.J., Harris D.E., Worrall D.M., Birkinshaw M., 2004, ApJ, 612, 729
Hardcastle M.J., Krause M.G.H., MNRAS, 430, 174
Heckman T.M., Lehnert M.D., Miley G.K., van Breugel W., 1991, ApJ, 370, 78
Heavens A.F., Meisenheimer K., 1987, MNRAS, 225, 335
Jaffe W.J., Perola G.C., 1973, A&A, 26, 423
Jamrozy M., Konar C., Machalski J., & Saikia D.J., 2008, MNRAS, 385, 1286
Jamrozy M., Konar C., Saikia D.J., Stawarz Ł., Mack K.-H., Siemiginowska A., 2007, MNRAS, 378, 581
Joshi S.A., Nandi S., Saikia D.J., Ishwara-Chandra C.H., Konar C., 2011, MNRAS, 414, 1397
Kaiser C.R., Alexander P., 1997, MNRAS, 286, 215
Kaiser C.R., Schoenmakers A.P., Röttgering H.J.A., 2000, MNRAS, 315, 381
Kirk J.G., Guthmann A.W., Gallant Y.A., Achterberg A., 2000, ApJ, 542, 235
Konar C., Jamrozy M., Hardcastle M.J., Croston J.H., Nandi S., Saikia D.J., Machalski J., 2011, JApA, 32, 477
Konar C., Hardcastle M.J., Jamrozy M., Croston C., Nandi S., 2012, MNRAS, 424, 1061
Konar C., Hardcastle M.J., Jamrozy M., Croston C., 2013, MNRAS, 430, 2137
Konar C., Saikia D.J., Jamrozy M., Machalski J., 2006, MNRAS, 372, 693
Kraft R.P., Hardcastle M.J., Worrall D.M., Murray S.S., 2005, ApJ, 622, 149
Laing R.A., Peacock J.A., 1980, MNRAS, 190, 903
Lal D.V., Rao A.P., 2007, MNRAS, 374, 1085
Landau L.D., Lifshitz E.M., 1966, Fluid Mechanics, 3rd Edition
Leahy J.P., Williams A.G., 1984, MNRAS, 210, 929
Liu F.K., Wu X.-B., Cao S.L., 2003, MNRAS, 340, 411
Machalski J., Jamrozy M., Konar C. 2010, A&A, 510, 84
McCarthy P. J., 1993, ARA&A, 31, 639
McNamara B.R., Nulsen P.E.J., 2012, NJPh, 14, e5023
Meisenheimer K., Röser H.-J., Hiltner P.R., Yates M.G., Longair M.S., Chini R., Perley R.A., 1989, A&A, 219, 63
Merritt D., Ekers R.D., 2002, Sci, 297, 1310
Mingo B., Hardcastle M.J., Croston J.H., Evans D.A., Kharb P., Kraft R.P., Lenc E., 2012, ApJ, 758, 95
Mullin L.M., Hardcastle M.J., 2009, MNRAS, 398, 1989

Nandi S., Pirya A., Pal S., Konar C., Saikia D.J., Singh M., 2010, MNRAS, 404, 433
Pacholczyk A.G., 1970, Radio Astrophysics, Freeman & Co., San Francisco
Paczyński B., Wiita P.J., 1980, A&A, 88, 23
Richstone et al., 1998, Nature, 395, 14
Rottmann H., 2001, PhD Thesis, University of Bonn
Safouris V., Subrahmanyan R., Bicknell G.V., Saripalli L., 2008, MNRAS, 385, 2117
Saikia D.J., Konar C., Kulkarni V.K., 2006, MNRAS, 366, 1391
Saripalli L., Mack K.-H., 2007, MNRAS, 376, 1385
Saripalli L., Subrahmanyan R., Udaya−Shankar N., 2002, ApJ, 565, 256
Scheuer P.A.G., 1995, MNRAS, 277, 331
Schoenmakers A.P., de Bruyn A.G., Röttgering H.J.A., van der Laan H., Kaiser C.R., 2000a, MNRAS, 315, 371
Schoenmakers A.P., de Bruyn A.G., Röttgering H.J.A., van der Laan H., 2000b, MNRAS, 315, 395
Shelton R.L., Kwak K., Henley D.B., 2012, ApJ, 751, 120
Synge J.L., 1957, The Relativistic Gas (Amsterdam: North-Holland)
Wilson A.S., Young A.J., Shopbell P.L., 2000, ApJ, 544, L27
Worrall D.M., Birkinshaw M., Cameron R.A., 1995, ApJ, 449, 93
Zier C., Biermann P.L., 2001, A&A, 377, 23

APPENDIX A: THEORETICAL ASPECTS OF MOMENTUM BALANCE

A1 Momentum balance at the jet heads

We consider a jet in the steady state (see Fig. 3). The momentum flow rate will remain conserved across the JTS as well as the contact discontinuity. Since the jet fluid is dominated by relativistic particles, it should be treated relativistically. Hereafter, all the quantities we use are proper quantities unless otherwise specified

We assume that the relativistic fluid description holds for the jet matter. For the momentum balance of the relativistic flow of the relativistic jet fluid at the hotspots, we start with the energy-momentum tensor (T^{ik}) which has the form

$$T^{ik} = wu^i u^k - Pg^{ik}, \tag{A1}$$

(Landau & Lifshitz 1966), where w is the enthalpy density; u^i is the ith component of the 4-velocity of the fluid, such that $u^0 = \Gamma.1$ (temporal component) and $u^\alpha = \Gamma\beta^\alpha$ (spatial comonents, $\beta = \frac{v}{c}$ is not the proper velocity); and g^{ik} is the metric tensor in flat space-time of the form

$$\begin{pmatrix} 1 & 0 & 0 & 0 \\ 0 & -1 & 0 & 0 \\ 0 & 0 & -1 & 0 \\ 0 & 0 & 0 & -1 \end{pmatrix} \tag{A2}$$

(i, k, α and 0 are not exponents, but indices to represents different components of the quantities).

$$w = e + P, \tag{A3}$$

where e is the relativistic internal energy density, P is the pressure of the jet fluid. In an explicit manner equation (A1) can be written as

$$\begin{pmatrix} \Gamma^2 e + \Gamma^2\beta^2 P & \Gamma^2 w\beta_x & \Gamma^2 w\beta_y & \Gamma^2 w\beta_z \\ \Gamma^2 w\beta_x & \Gamma^2 w\beta_x^2 + P & \Gamma^2 w\beta_x\beta_y & \Gamma^2 w\beta_x\beta_z \\ \Gamma^2 w\beta_y & \Gamma^2 w\beta_y\beta_x & \Gamma^2 w\beta_y^2 + P & \Gamma^2 w\beta_y\beta_z \\ \Gamma^2 w\beta_z & \Gamma^2 w\beta_z\beta_x & \Gamma^2 w\beta_z\beta_y & \Gamma^2 w\beta_z^2 + P \end{pmatrix}. \tag{A4}$$

Since the radio galaxy jets are collimated jets, the fluid motion can very well be approximated as one dimensional flow. Even though there must be velocity structure across the cross section of the jets, this is of no relevance to us, because the quantity of interest is the jet power ($Q_{\rm j}$) which is the time rate of flow of energy that passes through a cross-sectional area held fixed at the host galaxy frame and normal to the jet axis. Velocity structure, though it has been argued for in some models of jet emission processes, has so far not been constrained directly from observations.

The spatial part of T^{ij} will give us the momentum flow rate, which can be written as

$$T^{\delta\mu} = \Gamma^2 w\beta^\delta\beta^\mu + P\delta^{\delta\mu} \tag{A5}$$

For one dimensional flow, say in the x direction, we have to take the projection of the tensor along the x direction. The momentum flow rate (Π) in the x direction is given by

$$\Pi(x) =< x|\mathbf{T}|x >= T^{xx}, \tag{A6}$$

where $|x >$ is a unit bra-vector along the x direction, and $< x|$ is its ket-vector. $\mathbf{T}$ is the energy-momentum tensor. Since from equation (A4),

$$T^{xx} = \Gamma^2 w(\beta)^2 + P$$

(with β_x replaced by β), the momentum flow rate per unit area of jet cross section is as follows

$$\Pi(x) = (\Gamma_{\rm j}^2 w_{\rm j}\beta_{\rm j}^2 + P_{\rm j}) \tag{A7}$$

Following the treatment of Bicknell (1994), gravity, along with the buoyancy force and any entrained momentum in the jets can be neglected. We have assumed pressure-confined jets, and the jet pressure (P_j) and ambient medium pressure (P_a) are negligible compared to jet momentum flux. So the net momentum flow rate per unit cross sectional area is

$$\Pi_{\rm j}(x) = \Gamma_{\rm j}^2 w_{\rm j}\beta_{\rm j}^2 \tag{A8}$$

This is the momentum flow rate in the host galaxy frame.

In the hotspot frame (which is moving with a velocity of $\beta_{\rm hs}$ with respect to the host galaxy frame) the above expression will have the same form but the quantities will be replaced by those in the hotspot frame and can be written as $(\Gamma_{\rm j,hs}^2 w_{\rm j}\beta_{\rm j,hs}^2)A_{\rm j}$ (see Bicknell 1994 for a more regorous treatment). Thus, the momentum balance at the hotspot as seen in the hotspot frame can be written as

$$\Gamma_{\rm hs}^2 w_{\rm a}\beta_{\rm hs}^2\ A_{\rm h} = \Gamma_{\rm j,hs}^2 w_{\rm j}\beta_{\rm j,hs}^2\ A_{\rm j} \tag{A9}$$

We know that the the particles in the jets are accelerated in the hotspots and thereby inflate lobes whose internal pressure is similar to the external (or ambient medium) pressure (Croston et al. 2004; Konar et al., 2009; Shelton, Kwak & Henley, 2012). In relativistic dynamics, the enthalpy contains a term accounting for the rest mass energy. We can thus write w, for both the jet fluid and ambient medium fluid, as

$$w = \rho^0 c^2 + \epsilon + P = \rho c^2 + P, \tag{A10}$$

where ρ is the proper density of the magnetised thermal/nonthermal matter and can be expressed as

$$\rho = \rho^0 + \frac{\epsilon}{c^2}. \tag{A11}$$

Relating the quantities in the host galaxy frame and the hotspot frame using velocity addition theory it can be shown that

$$\Gamma_{\rm j,hs}^2\beta_{\rm j,hs}^2 = \Gamma_{\rm j}^2\Gamma_{\rm hs}^2(\beta_{\rm j} - \beta_{\rm hs})^2. \tag{A12}$$

The jet power ($Q_{\rm j}$) as measured in the host galaxy frame can be expressed as

$$Q_{\rm j} = \Gamma_{\rm j}^2 w_{\rm j}(\beta_{\rm j} c) A_{\rm j}, \tag{A13}$$

where $Q_{\rm j}$ includes the rest mass energy of the jet matter.

Replacing $\Gamma_{\rm j,hs}^2\beta_{\rm j,hs}^2$ from equation (A12) into equation (A9) and then replacing $\Gamma_{\rm j}^2 w_{\rm j} A_{\rm j}$ from equation (A13), the momentum balance equation becomes

$$\frac{Q_{\rm j}}{\beta_{\rm j} c} = w_{\rm a} A_{\rm h} (\frac{\beta_{\rm hs}}{\beta_{\rm j} - \beta_{\rm hs}})^2. \tag{A14}$$

This can be rearranged to give

$$\beta_{\rm hs} = \left(\frac{1}{1+\eta}\right)\beta_{\rm j}, \tag{A15}$$

where

$$\eta = \sqrt{\left(\frac{\beta_{\rm j} c A_{\rm h} w_{\rm a}}{Q_{\rm j}}\right)} \tag{A16}$$

APPENDIX B: ALGEBRAIC EXPRESSIONS OF SOME PARAMETERS IN THE EXPRESSIONS OF FAST AND SLOW WAVES

According to Chou & Hao (2004), the fast and slow waves in a relativistic magnetoplasma, which exerts isotropic pressure, can be given by

$$V_{\rm f,s}^2 = \frac{-b_{\rm is} \pm \sqrt{b_{\rm is}^2 - 4a_{\rm is}C_{\rm is}}}{2a_{\rm is}}, \tag{B1}$$

where $a_{\rm is}$, $b_{\rm is}$ and $C_{\rm is}$ are given below.

$$a_{\rm is} = 1 + \frac{1}{\rho^0 c^2}\left(\frac{B^2}{4\pi} + 2P^{\rm nt} + 2\epsilon^{\rm nt}\right) + \frac{1}{(\rho^0 c^2)^2}\left\{(\epsilon^{\rm nt} + P^{\rm nt})^2 + (\epsilon^{\rm nt} + P^{\rm nt})\frac{B^2}{4\pi}\right\}, \tag{B2}$$

$$b_{\rm is} = \frac{1}{\rho^0}(\gamma_{\rm ad} P^{\rm nt} + \frac{B^2}{4\pi}) + \frac{1}{\rho^{0 2} c^2}\left\{(\gamma_{\rm ad} P^{\rm nt} + \frac{B^2}{4\pi})(\epsilon^{\rm nt} + P^{\rm nt}) + (\gamma_{\rm ad} P^{\rm nt})(\frac{B^2}{4\pi})\cos^2\theta\right\} \tag{B3}$$

and

$$C_{\rm is} = \frac{\gamma_{\rm ad} P^{\rm nt}}{\rho^{0 2}}\frac{B^2}{4\pi}\cos^2\theta. \tag{B4}$$

In the limit $\rho^0 c^2 \to 0$, $a_{\rm is}$ and $b_{\rm is}$ blow up. Since we have to deal with $\rho^0 c^2 \to 0$ limit, we better work with $b^{'}$ and $C^{'}$, where

$$b^{'} = \frac{b_{\rm is}}{a_{\rm is}} = \frac{(\gamma_{\rm ad} P^{\rm nt} + \frac{B^2}{4\pi})\rho^0 c^2 + (\gamma_{\rm ad} P^{\rm nt} + \frac{B^2}{4\pi})(\epsilon^{\rm nt} + P^{\rm nt}) + (\gamma_{\rm ad} P^{\rm nt})(\frac{B^2}{4\pi})\cos^2\theta}{(\rho^0 c^2)^2 + (\frac{B^2}{4\pi} + 2P^{\rm nt} + 2\epsilon^{\rm nt})\rho^0 c^2 + (\epsilon^{\rm nt} + P^{\rm nt})(\epsilon^{\rm nt} + P^{\rm nt} + \frac{B^2}{4\pi})} c^2 \tag{B5}$$

and

$$C^{'} = \frac{C_{\rm is}}{a_{\rm is}} = \frac{(\gamma_{\rm ad} P^{\rm nt})(\frac{B^2}{4\pi})\cos^2\theta}{(\rho^0 c^2)^2 + (\frac{B^2}{4\pi} + 2P^{\rm nt} + 2\epsilon^{\rm nt})\rho^0 c^2 + (\epsilon^{\rm nt} + P^{\rm nt})(\epsilon^{\rm nt} + P^{\rm nt} + \frac{B^2}{4\pi})} c^4. \tag{B6}$$

In the limit $\rho^0 c^2 \to 0$, even if $a_{\rm is}$ and $b_{\rm is}$ blows up, $b^{'}$ and $C^{'}$ does not. Therefore, just replacing $\rho^0 c^2$ by zero, we will get the expression for $V_{\rm I}$, $V_{\rm f}$ and $V_{\rm s}$ in the ultrarelativistic limit.

APPENDIX C: ESTIMATION OF MASS AND SPIN ACCUMULATION OF SUPERMASSIVE BLACK HOLE DURING QUISCENT PHASE

C1 Mass accumulation

If we assume that the SMBH accretes and radiates at a constant fraction of the Eddington rate in the quiescent phase, we can write

$$L_{\rm bol} = \lambda L_{\rm Edd}, \tag{C1}$$

where $L_{\rm bol}$ is bolometric luminosity and $L_{\rm Edd}$ is the Eddington luminosity. If the radiative efficiency factor is ξ, then the mass accretion rate is

$$\dot{M} = \frac{L_{\rm bol}}{\xi c^2}. \tag{C2}$$

Application of equations (C1) and (C2) yields

$$\Delta M = \int_0^{\Delta t} \dot{M} dt = \frac{\lambda}{\xi}\frac{L_{\rm Edd}}{c^2}\Delta t \tag{C3}$$

Expressing in astronomical units, equation (C3) becomes

$$\left(\frac{\Delta M}{M_\odot}\right) = 2.27 \times 10^{-9}\left[\frac{\lambda}{\xi}\left(\frac{M_\bullet}{M_\odot}\right)\left(\frac{\Delta t}{\rm yr}\right)\right], \tag{C4}$$

where $M_\odot$ is solar mass.

C2 Spin accumulation

We use the Newtonian physics for our crude estimate just to have an idea about the situation. The specific orbital angular momentum of the disk matter at ISCO is given by

$$J = V_k 3R_s = \sqrt{GM_\bullet 3R_s} = \sqrt{6}\frac{GM_\bullet}{c}, \tag{C5}$$

where V_k is the Keplerian speed (substituting in for R_s). When the matter is accreted onto the black hole, the orbital angular momentum of the matter adds to the spin angular momentum, $S_\bullet$ of the black hole. The total change in angular momentum, Λ, over the time Δt can be expressed as

$$\Delta\Lambda = \pm J \times \Delta M,$$

where $+$ and $-$ sign are for a co-rotating and counter-rotating disk with respect to the black hole spin. Substituting the expression of ΔM from equation (C3), we obtain

$$\Delta\Lambda = \pm\frac{\sqrt{6}GM_\bullet}{c} \times \frac{\lambda}{\xi}\frac{L_{\rm Edd}}{c^2}\Delta t \tag{C6}$$

We can calculate the increase in the dimensionless angular momentum parameter, a which is given by

$$a = \frac{S_\bullet c}{GM_\bullet^2}. \tag{C7}$$

The change in a is the total orbital angular momentum (in dimensionless units) of the accreted matter, and is given by

$$\Delta a = \pm\frac{(\Delta\Lambda)c}{GM_\bullet^2}.$$

Substituting $\Delta\Lambda$ from equation (C6), we obtain

$$\Delta a = \pm\sqrt{6}\frac{\lambda}{\xi}\frac{L_{\rm Edd}}{M_\bullet c^2}(\Delta t) \tag{C8}$$

Replacing $L_{\rm Edd} = 1.3\times10^{38}(\frac{M_\bullet}{M_\odot})$ erg s^{-1} and expressing Δt in yr, the above expression can be written as

$$\Delta a = \pm\sqrt{6}\frac{\lambda}{\xi}\frac{4.1\times10^{45}}{M_\odot c^2}(\frac{\Delta t}{\rm yr}) \tag{C9}$$

This expression is independent of $M_\bullet$. With the same canonical values of λ and ξ, for the duration of quiescent phase, $\Delta t = 10^7$ yr,

$$\Delta a = \pm0.056 \tag{C10}$$

Since, we have assumed that the ISCO is at $3R_s$, we can use pseudo General Relativistic (GR) potential (Paczyński & Wiita 1980) to estimate values of V_k to get the better estimation of Δa. Equating gravitational force with the centrifugal force we get the following expression of the specific angular momentum:

$$J = V_k r = \sqrt{GM_\bullet r}\left(\frac{r}{r-R_s}\right). \tag{C11}$$

Replacing $r = 3R_s$, we get

$$J = \sqrt{GM_\bullet 3R_s}\frac{3}{2} \tag{C12}$$

In the validity regime of the pseudo-GR potential, the Newtonian expression of Δa (equation C9) should be multiplied by a factor of $\frac{3}{2}$. The GR-corrected expression should therefore be

$$\Delta a = \pm\sqrt{6}\frac{\lambda}{\xi}\frac{6.15\times10^{45}}{M_\odot c^2}(\frac{\Delta t}{\rm yr}). \tag{C13}$$

This gives us

$$\Delta a = 0.056\times\frac{3}{2} = 0.084. \tag{C14}$$

APPENDIX D: RATIO OF INTERNAL ENERGY DENSITY TO KINETIC ENERGY DENSITY OF THE JET FLUID IN THE SPINE OF THE JET

The kinetic energy ($e_{\rm ke,j}$) content per unit proper volume of the jet is given by

$$e_{\rm ke,j} = \Gamma_{\rm j}(\Gamma_{\rm j}-1)\rho_{\rm j}^0 c^2 + \Gamma_{\rm j}(\Gamma_{\rm j}-1)(\epsilon_{\rm j}+P_{\rm j})$$

$$= \Gamma_{\rm j}(\Gamma_{\rm j}-1)[\rho_{\rm j}^0 c^2 + \gamma\epsilon_{\rm j}],$$

we have used the relation $P_{\rm j} = (\gamma-1)\epsilon_{\rm j}$, where γ is the adiabatic index and $\epsilon_{\rm j}$ is the internal energy (without the rest mass energy) density of the jet fluid. With a little algebra, we obtain

$$\epsilon_{\rm j} = \frac{1}{\Gamma_{\rm j}(\Gamma_{\rm j}-1)\gamma\left[1+\frac{1}{\gamma}\chi_{\rm j}\right]}e_{\rm ke,j}, \tag{D1}$$

where $\chi_{\rm j} = \frac{\rho_{\rm j}^0 c^2}{\epsilon_{\rm j}}$.

Whatever the EoS of the jet fluid may be, the adiabatic index γ must obey the inequality $\frac{4}{3} \le \gamma \le \frac{5}{3}$. So γ is always > 1. Therefore, whatever the value of $\chi_{\rm j}$ ($\chi_{\rm j} > 0$) for FR II jets, the quantity within the bracket in the denominator of equation (D1) is greater than 1. So, for any value of $\Gamma_{\rm j} > 1$, $\epsilon_{\rm j} < e_{\rm ke,j}$. Now if we are to believe X-ray inverse-Compton studies (e.g. Hardcastle 2006) that argue that $\Gamma_{\rm j} > 15$ for the spine of the jet, then we can safely conclude that $\epsilon_{\rm j} \ll e_{\rm ke,j}$, and hence the internal energy content of the pre JTS jet fluid is negligible compared to the bulk kinetic energy of the jet fluid. Even for a more modest value of $\Gamma_{\rm j} = 4$, which is not an absurd value for the jet spine, $\epsilon_{\rm j}$ is lower than $e_{\rm ke,j}$ by a factor that is greater than ~ 12.